

**Energetic Interactions Within the Solid-State Spectrometer of the ASCA  
Satellite**

by  
Srimal Wangu

Submitted to the  
Department of Physics and the Department of Electrical Engineering and Computer Science  
in Partial Fulfillment of the Requirements for the Degrees of

Bachelor of Science in Physics  
Bachelor of Science in Electrical Science and Engineering  
and Master of Engineering in Electrical Engineering and Computer Science  
at the Massachusetts Institute of Technology

May 1995

[JUNE 1995]

© 1995 Srimal Wangu. All rights reserved.

The author hereby grants to M.I.T. permission to reproduce  
and to distribute copies of this thesis document in whole or in part,  
and to grant others the right to do so.

Signature of Author \_\_\_\_\_

\_\_\_\_\_   
 May 25, 1995

Certified by \_\_\_\_\_

Mildred S. Dresselhaus  
Thesis Supervisor

Accepted by \_\_\_\_\_

Aron Bernstein  
Department of Physics Undergraduate Theses Coordinator

Accepted by \_\_\_\_\_

F.R. Morgenthaler  
Chairman, Department Committee on Undergraduate Theses  
MASSACHUSETTS INSTITUTE  
OF TECHNOLOGY

AUG 10 1995

Energetic Interactions Within the Solid-State Spectrometer of the ASCA Satellite

by

Srimal Wangu

Submitted to the

Department of Physics

and the Department of Electrical Engineering and Computer Science

May 1995

In Partial Fulfillment of the Requirements for the Degrees of

Bachelor of Science in Physics

Bachelor of Science in Electrical Science and Engineering

and Master of Engineering in Electrical Engineering and Computer Science

**ABSTRACT**

ASCA is a broad band (0.3 - 12 keV) x-ray astrophysical observatory in which various instruments operate with high throughput and high spectral resolution. Detailed examination of the method in which photoelectronic interactions occur in the Charge Coupled Devices (CCDs) of the Solid-State Imaging Spectrometer (SIS) on ASCA reveals a sudden variation in the nearly linear CCD signal output versus energy input curve near the silicon K-edge. The focus of this thesis is the modeling of the behavior of the SIS CCD at the silicon K-edge, first by theoretical analysis, and then by analysis of X-ray spectral data already acquired from the instrument. The relationship between CCD signal out and incoming photon energy at the silicon K-edge in the ASCA detectors is studied in detail in order to define and analyze the behavior of the CCD in this range.

The results from this study showed that theoretically, a one to two percent deviation between incoming energy and output pulseheight should exist in the CCD. Although the nonlinearity was consistent with the available data, insufficient signal-to-noise in this data restricted the definite quantification of this disparity.

Thesis Supervisor: Mildred S. Dresselhaus

Title: Institute Professor

# Table of Contents

Introduction .....	7
1.2 Purpose of this Research .....	13
Technical and Theoretical Background .....	15
2.1 X-Ray Detectors .....	15
2.2 Measurement of CCD Output Pulseheight versus Expected Output Energy.	22
CCD Efficiency .....	22
ASCA/SIS Grades and Pulseheight Calculations .....	24
2.3 Theoretical Analysis of X-Ray Induced Charge Cloud	
Diffusion .....	29
Investigation of Energetic Interactions Within the SIS .....	38
3.1 The Spectrometer and the Dispersion Solution .....	38
3.2 SIS CCD Analysis .....	50
CCD Frame Rotation .....	50
Final Analysis .....	52
3.3 Results of Analysis .....	62
Conclusion .....	66
Appendices .....	68
Appendix A: Results from the Fraser, et al. Calculation .....	68
Appendix B: Henke Scattering Factors .....	69
Appendix C: Filtering and Rotation programs .....	71
Appendix D: Averaging Programs .....	76
References .....	82

# List of Figures

- Figure 1.1.1.** Drawing of the ASCA satellite (*Astro-D Technical Description, AO-1 version*)
- Figure 1.1.2.** On-axis effective area of ASCA as a function of Energy. Effective areas of the Einstein and AXAF satellites are shown for comparison. (*Tanaka*)
- Figure 1.1.3.** ASCA's focal plane instruments: the GIS and the SIS. (*Astro-D Technical Description, AO-1 version*)
- Figure 1.1.4.** Comparison of the fields of view of the GIS and the SIS. (*Inoue*)
- Figure 1.2.1.** Comparison of expected output pulseheight versus pulseheight from CCD simulator.
- Figure 2.1.1.** Schematic representation of the p-n junction.
- Figure 2.1.2.** Configuration of the SIS CCD chips. (*Astro-D Technical Description, AO-1 version*)
- Figure 2.1.3.** Schematic of SIS CCD gate structure (NOT TO SCALE). (*Bautz*)
- Figure 2.1.4.** Lincoln Lab CCD pulseheight distributions (found for a few characteristic K-lines). (*Inoue*)
- Figure 2.1.5.** Distribution of impinging photons within the CCD.
- Figure 2.2.1.** CCD efficiency (%) vs. Photon energy (eV)
- Figure 2.2.2.** Photoelectric absorption of an x-ray photon.
- Figure 2.2.3.** Various types of ASCA grades. (*Astro-D Technical Description, AO-1 version*)
- Figure 2.3.1.** Comparison of charge cloud sizes for different input energies.
- Figure 3.1.1.** Typical CCD frame of data.
- Figure 3.1.2.** Schematic diagram of the spectrometer.
- Figure 3.1.3.** Output pulseheight vs. y coordinate, noting a few spectral "lines" or peaks.
- Figure 3.1.4.** Fitting the data in order to determine the dispersion solution of the spectrometer.
- Figure 3.2.1.** Theoretical expected form of  $\Delta E$  vs. y plot.

**Figure 3.2.2.**  $\Delta E$  vs.  $y$  for all single event points.

**Figure 3.2.3.** Cumulative plot of averaged  $\Delta E$  vs.  $y$ , averaged every single  $y$  value.

**Figure 3.2.4.** Cumulative plot of averaged  $\Delta E$  vs.  $y$ , averaged every five  $y$  values.

**Figure 3.2.5.** Cumulative plot of averaged  $\Delta E$  vs.  $y$ , averaged every ten  $y$  values.

**Figure 3.2.6.** Gaussian fit to histograms of every ten  $y$  values.

# Chapter 1

## Introduction

### 1.1 The Advanced Satellite for Cosmology and Astrophysics

The Advanced Satellite for Cosmology and Astrophysics (ASCA) is a joint US-Japan mission. ASCA (formerly called Astro-D) provides a unique capacity to address many of the practical problems of x-ray astronomy.

ASCA was launched on February 20, 1993 on a Japanese M-3SII launch vehicle into an approximately circular orbit with an altitude of 520 to 620 kilometers and an inclination of about 31.5 degrees. This 417 kilogram satellite is three-axis stabilized, with an absolute pointing accuracy of about 10 arcseconds. [FIGURE 1.1.1]

ASCA's advanced capabilities are, first, the fact that it is the first x-ray astronomy satellite able to image in the broad band (0.3 to 12 keV) range and, second, the fact that it has a few unique features: good energy resolution and high throughput over a wide energy range.

ASCA is capable of “moderate angular resolution”, i.e. it can resolve stellar sources to approximately one arcminute. ASCA is equipped with four nested thin-foil telescopes which work together to provide a large effective area over a wide energy range; for the four telescopes, the effective area is approximately 1300 cm<sup>2</sup> for energies less than one keV, and approximately 600 cm<sup>2</sup> in the six to seven keV range. [FIGURE 1.1.2] In addition to

a large effective area, ASCA has a relatively long focal length of 3.5 meters which was attained by deploying an extendable optical bench once in orbit.

Aboard ASCA, the four conical-foil telescopes illuminate two different types of detectors, the Solid-State Imaging Spectrometer (SIS), and the Gas Imaging Spectrometer (GIS), which operate independently and simultaneously. Both the Charge Coupled Device (CCD) cameras of the SIS and the imaging gas scintillation proportional counters (IGSPC) of the GIS are used as focal plane instruments. [FIGURE 1.1.3]

The Gas Imaging Spectrometer on ASCA is characterized by its high background (non x-ray signal) rejection rate and its high resolution; the spectrometer has energy resolution of 8% and position resolution of 0.5 mm for 5.9 keV photons. The field of view of this instrument is circular, with a radius of twenty-five arcminutes. It is able to observe four times more area than its solid-state counterpart. [FIGURE 1.1.4]

The Solid-state Imaging Spectrometer on ASCA was constructed jointly by a team at MIT's Center for Space Research and a Osaka University/ISAS team. The SIS has a field of view of 22x22 arcminutes, and is characterized by excellent energy resolution (2% for 5.9 keV x-rays) which has been confirmed in orbit. The SIS is a powerful instrument for studying spectroscopic lines of oxygen through nickel. Therefore, ASCA is the first satellite in orbit which is able to operate with high throughput and high spectral resolution simultaneously, while covering a wide range of energies.

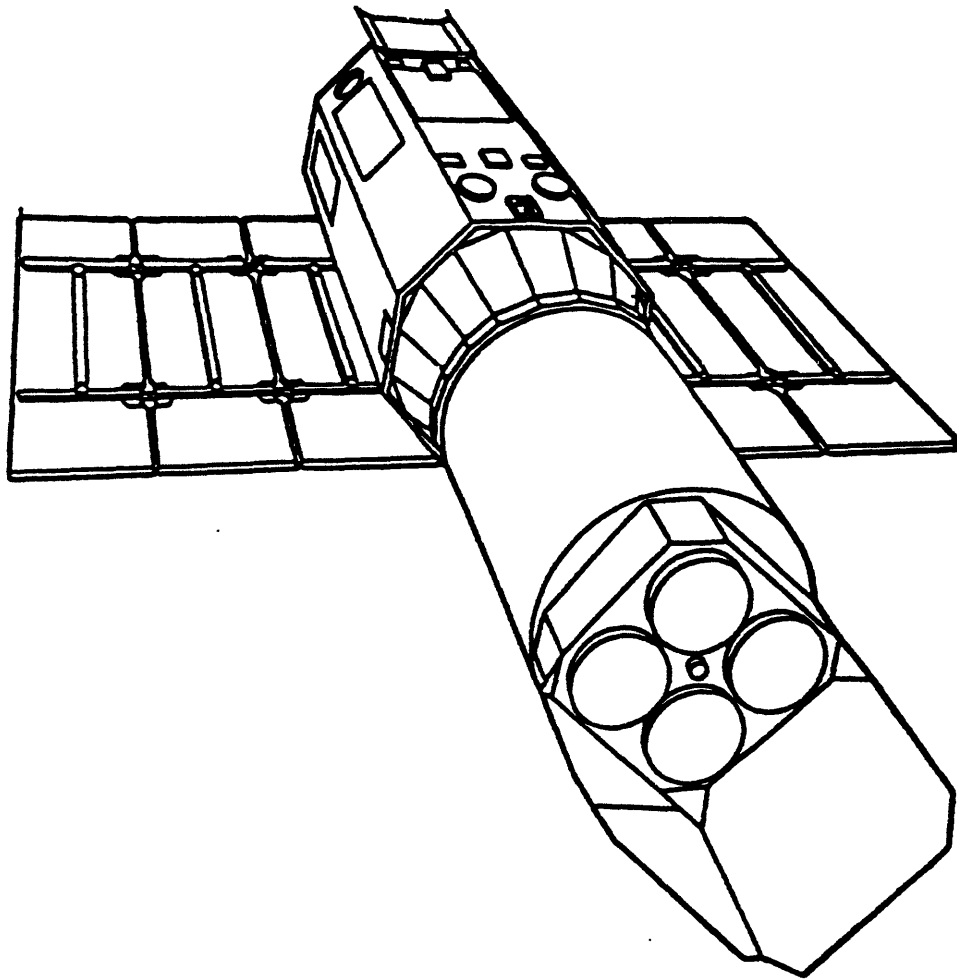


**Figure 1.1.1.** Drawing of the ASCA satellite (*Astro-D Technical Description, AO-1 version*)



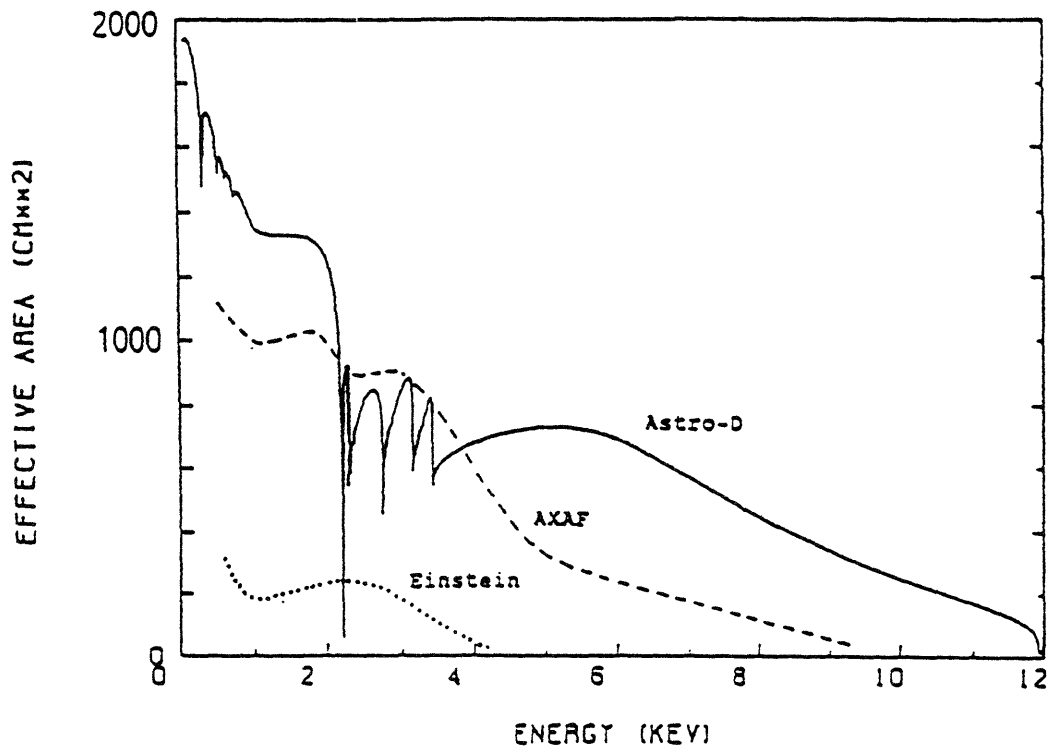
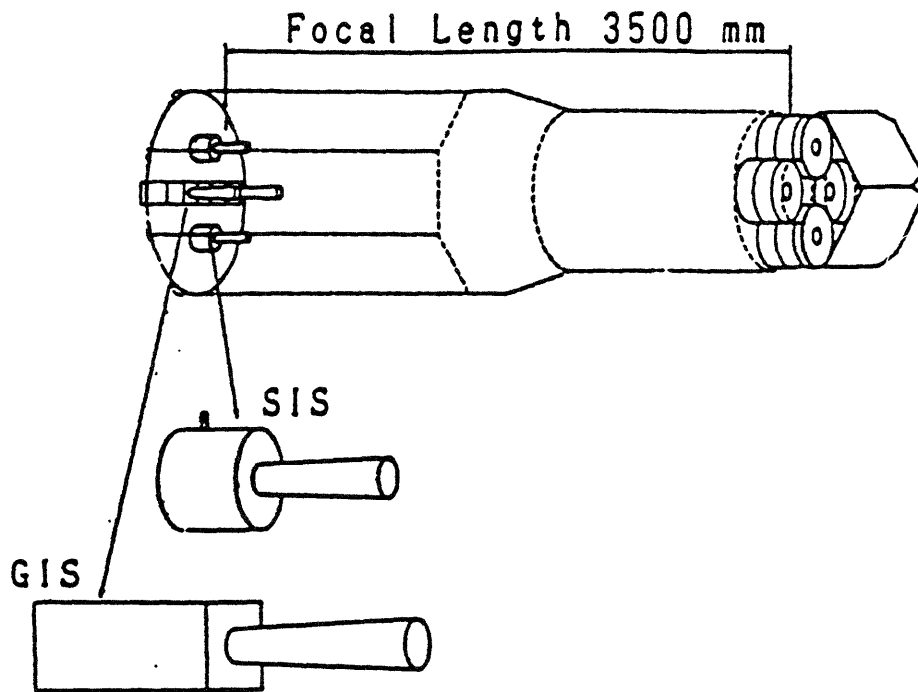
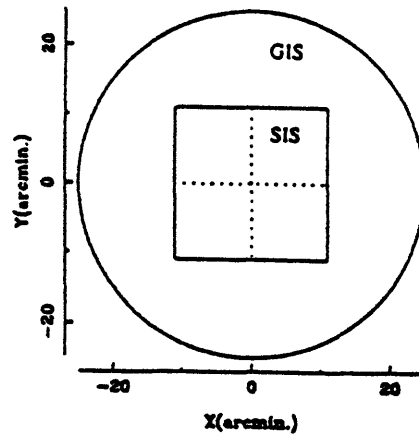


Figure 1.1.2. On-axis effective area of ASCA as a function of Energy. Effective areas of the Einstein and AXAF satellites are shown for comparison. (Tanaka)



**Figure 1.1.3.** ASCA's focal plane instruments: the GIS and the SIS. (*Astro-D Technical Description, AO-1 version*)



**Figure 1.1.4.** Comparison of the fields of view of the GIS and the SIS. (*Inoue*)

## 1.2 Purpose of this Research

The SIS is the first CCD x-ray spectrometer in orbit. For this reason, much can be learned from its performance. One potential problem with using a Solid-State detector is that we may find some non-linearities in the detector response due to sudden changes in photosensitive volume sampling. These non-linearities may create errors in the data produced by the SIS. Therefore, it is necessary and worthwhile to examine the behavior of the SIS detector at energies close to the characteristic energies of the materials of which the detector is built.

The focus of this research is the examination of the response of the silicon CCDs of the SIS across the silicon K-edge (1.840 keV). If we examine the relationship between the charge deposited on the CCD surface and the “pulseheight” values output by the CCD, we see a discontinuity at the K-edge energy. The existence of the discontinuity is directly related to the fact that a discontinuous change in absorption cross-section causes the mean free path of impinging photons to change suddenly for photons above and below this energy. This fact, coupled with the classification of photon “events” by ASCA scientists and the limited size of CCD pixels, causes charge to be lost discontinuously at the K-edge.

Using Andrew Rasmussen’s simulator program (MIT CSR, 1994) which models the SIS CCD by producing sample output pulseheight values for given input energies, we can predict the existence of a disparity between expected pulseheight due to input photon energy and the modeled “actual” pulseheight for energies less than 1.840 keV. We can see that the pulseheight read out by the CCDs is less than the original amount of charge deposited on the surface for energies at and below the silicon K-edge. [FIGURE 1.2.1]

What is the origin of and reason for this disparity? Can this disparity be isolated, analyzed, and quantified? This thesis attempts to answer these questions.

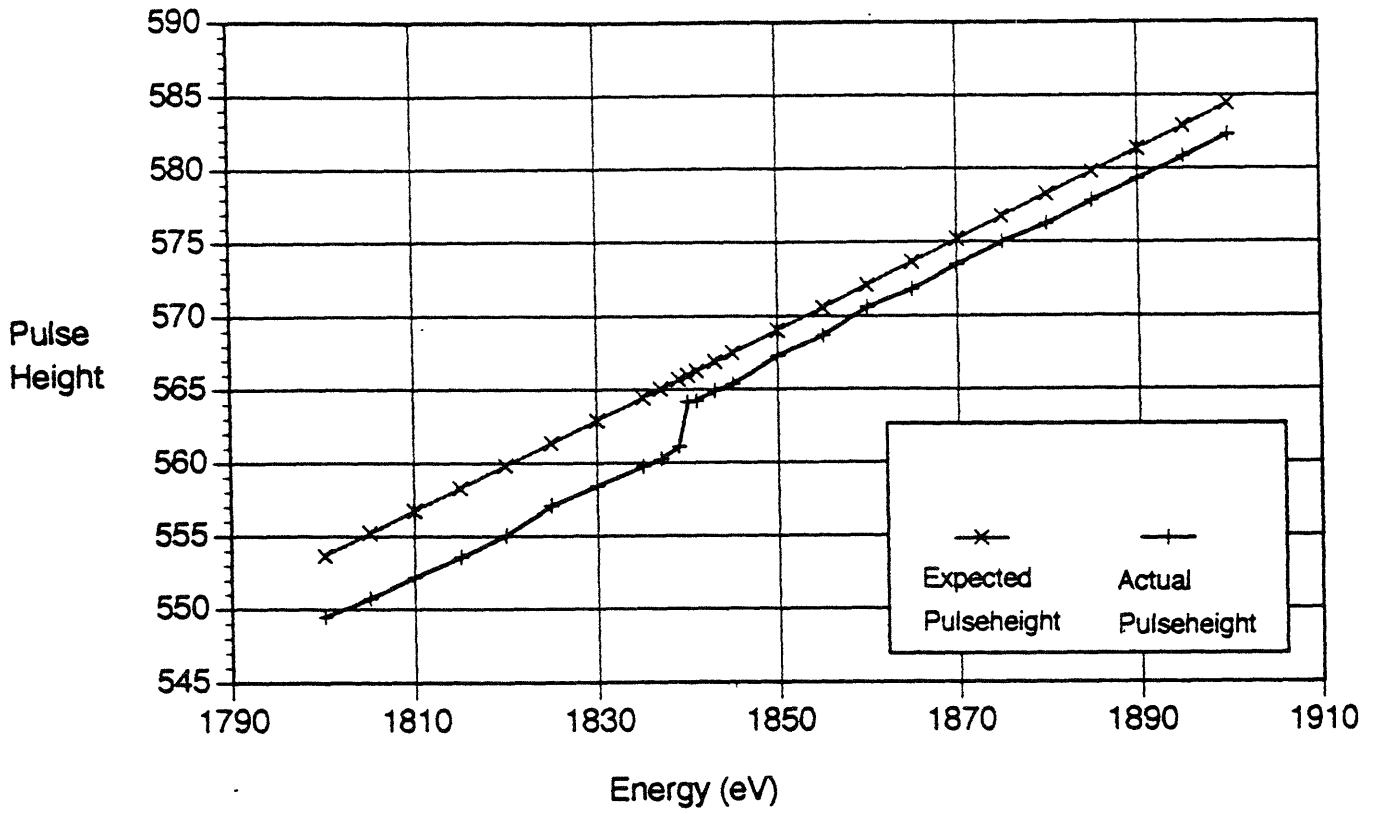


**Figure 1.2.1.** Comparison of Expected pulseheight vs. Pulseheight determined from CCD simulator.

## Chapter 2

# Technical and Theoretical Background

### 2.1 X-Ray Detectors

The SIS detectors on ASCA consist of two identical X-Ray cameras which use silicon-based CCDs. A CCD is a position sensitive electronic device which is not only able to determine the interaction point of a photon, but is also able to measure the photon's energy (in the case of X-ray interactions). The CCD x-ray detector is a relatively new technology; other types of detectors have been commonly used in the past.

The CCD belongs to a larger class of detectors called semiconductor ionization detectors. The semiconductor ionization detector has become popular in recent years due to its excellent energy resolution, low readout noise, and low output capacitance. Most semiconductor ionization devices are fabricated from germanium or silicon. They are characterized by the p-n junction, based on a single crystal in which a change in the doping level (or charge carrier concentration) and sign of charge carrier occurs over a short distance. [FIGURE 2.1.1]

In the area of the junction there are no free charge carriers. This region is called the depletion region. When a voltage is applied across the depletion region (as shown in the figure), the p and n charge carriers move in opposite directions away from the junction, and only a very small intrinsic current flows in the device. If the polarity of the voltage is reversed, the majority charge carriers flow across the junction. Therefore the p-n junction

acts as a “current rectifier”. In detector form, the p-n junction can be used as a “charge trap”: an x-ray photon hitting the surface of a semiconductor device will induce a charge in the device. This charge will be accumulated in the p-n junction and then can be made to flow out of the junction, for measurement by an amplifier.

In a similar way, an idealized CCD x-ray detector functions as follows: As an x-ray impinges upon the CCD, many primary electrons are created. As these electrons interact with others and lose energy, the energy loss of the primary electron goes to form a secondary electron and an electron hole pair which has the energy of the semi-conductor bandgap and some kinetic energy. The “cloud” of electron-hole pairs which is formed in this manner can be seen as a signal charge which has accumulated in the “buried” region of the CCD. The charge in this cloud is proportional to the energy of the original incident x-ray. The depletion region carries an electric field which causes the cloud to drift into a potential well (called the charge transfer channel) which exists between the “buried channel” in the CCD structure and the depletion layer of the CCD. After certain fixed intervals of time, voltage is applied to the CCD in pulses. In this manner, the charge is transferred all the way to the edge of the CCD array through the charge transfer channel, and then is read out by an output amplifier and measured before the electrons and holes recombine. Thus, the spatial position and original energy of the incident x-ray photon can be determined with accuracy.

The semiconductor detector is able to achieve highly accurate energy resolution because of the large number of electron-hole pairs eventually created in the depletion region. Due to this, the CCD/amplifier combination output can produce a complete, detailed spectrum of the incoming x-rays.

The Solid-State Imaging Spectrometer (SIS) on ASCA consists of four MIT Lincoln Laboratory 420x420 pixel CCD chips, abutted side-by-side (and read out by separate pre-amps). [FIGURE 2.1.2] These CCDs have a “layered” structure. At the

surface of the CCD are electrodes. These control the charge transfer for the device. Beneath the electrodes is an insulation layer, which covers the buried channel of the CCD. An electric field can be applied across the buried channel in order to make charge transfer possible. The electric field creates a depletion layer which extends to a depth of 35  $\mu\text{m}$ . Under the depletion layer is a base, or substrate, layer. Finally, on the bottom surface of the CCD is a backside diode which helps to eliminate stray charge which may accumulate outside of the buried channel. [FIGURE 2.1.3]

The energy resolution of the SIS CCDs is a function of the read-out noise of the detector, the energy of the incoming x-ray photons, the Fano factor (a constant which is approximately equal to 0.12), and dark current. Since the CCD is cooled to a temperature of  $-60^\circ\text{C}$ , thermal noise can be kept to a minimum. Therefore, the best possible result for the full-width half-maximum (FWHM) resolution (for a single event, in which all electrons are absorbed in one pixel) is

$$\Delta E_{\text{FWHM}} \approx 3.65 \cdot \sqrt{8 \ln 2} \cdot \sqrt{N^2 + \frac{FE}{3.65}}$$

where E is the incoming X-ray energy, N is the read-out noise of the SIS pre-amplifier, and F is the Fano factor. This means that the lower tolerance limit of the calculation of the output pulseheight from the CCD corresponds to this  $\Delta E_{\text{FWHM}}$ . Like most semiconductor detectors, the SIS exhibits excellent energy resolution; characteristic K-alpha and K-beta peaks in the x-ray spectrum are clearly distinct in the pulseheight distribution. [FIGURE 2.1.4]

The SIS CCDs function in a similar manner to the idealized description given above; when an x-ray hits the surface of the CCD, it creates one electron-hole pair per 3.65 eV of energy. This "quantum" of energy produced per electron is W, the electron gain of the CCD.



If the photon is absorbed in the depletion layer of the CCD, it is moved into the charge transfer channel, collected at the junction, and eventually transferred out and detected. However, if the photon has a large amount of energy, it may create a widespread cloud in the CCD substrate. This background noise will be detected and eliminated by the backside diode. [FIGURE 2.1.5] Another important difference between the actual CCD and the idealized model is that in the actual device, the induced charge cloud may diffuse into surrounding pixels. In other words, the limited pixel size of the CCD may result in some input charge not being recovered in the output of the CCD.

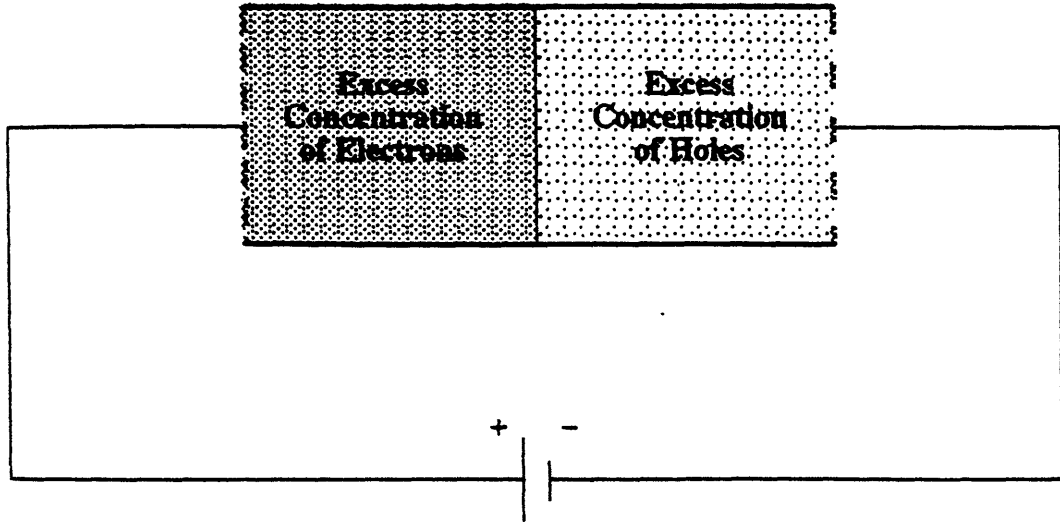


Figure 2.1.1. Schematic representation of the p-n junction.

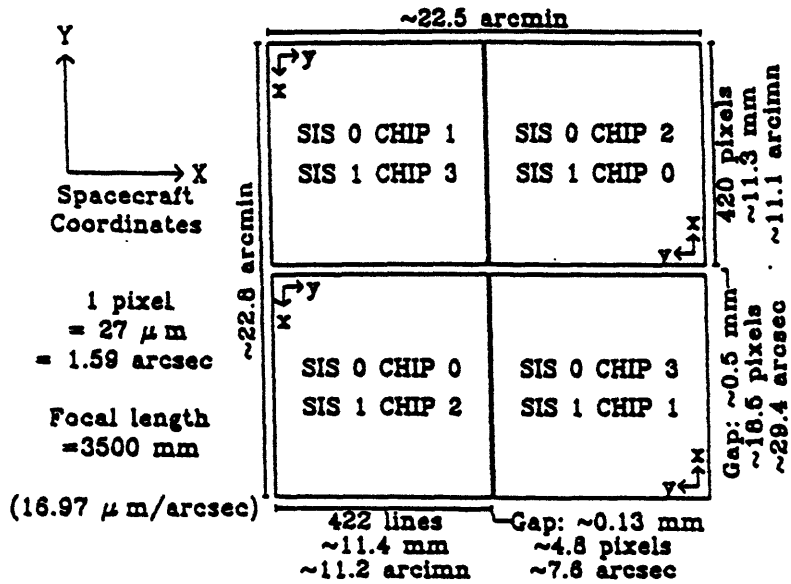
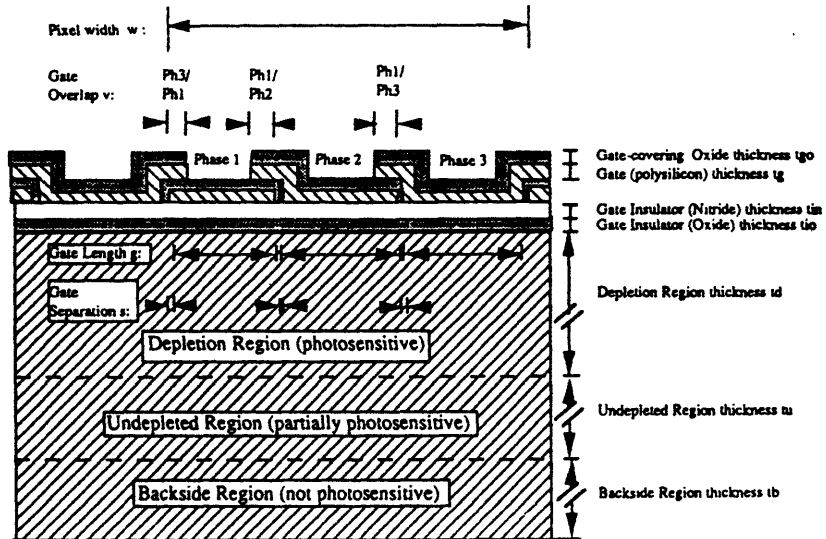
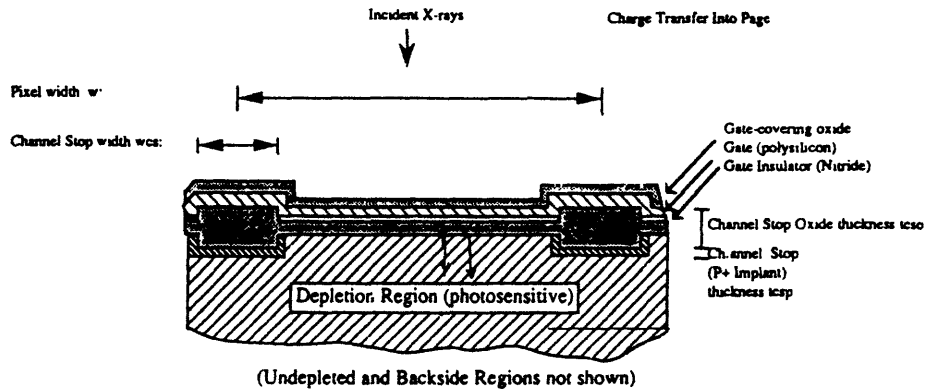


Figure 2.1.2. Configuration of the SIS CCD chips. (*Astro-D Technical Description, AO-1 version*)



Material Key:	
	Si O <sub>2</sub>
	Si <sub>3</sub> N <sub>4</sub>
	Si (polycrystalline)
	Si (monocrystalline)
	Si (p+, monocrys.)

Figure 2.1.3. Schematic of SIS CCD gate structure (NOT TO SCALE). (Bautz)

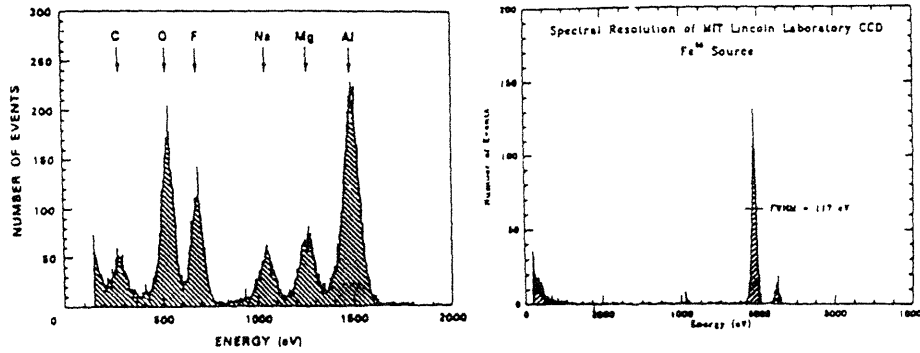


Figure 2.1.4. Lincoln Lab CCD pulseheight distributions (found for a few characteristic K-lines. *(Inoue)*)

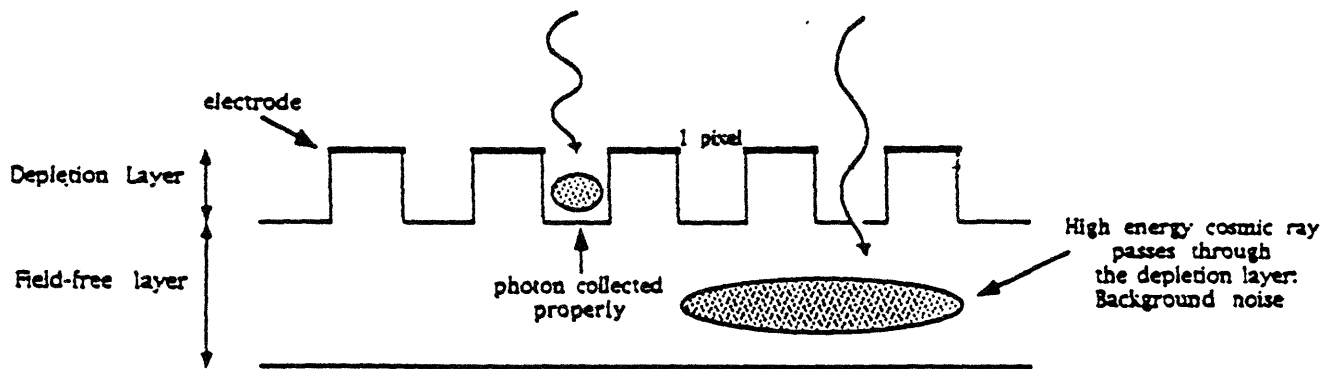


Figure 2.1.5. Distribution of impinging photons within the CCD.

## **2.2 Measurement of CCD Output Pulseheight versus Expected Output Energy**

If we once again examine in detail the way in which x-ray interactions occur in the CCD, we see that an x-ray photon travelling into the device may produce one energetic primary photoelectron and a cascade of secondary electrons. The number of electrons in this cascade is proportional to the energy of the original photon, and eventually it is the charge of this electron cloud which is approximated when the detector is read out.

Ideally, the photon energy impinging upon the detector should be exactly proportional to the magnitude of the electron cloud measured by the output pre-amplifier. However, if we specifically examine the relationship between the energy of the impinging x-ray and the CCD charge out in a given pixel, we see that diffusion of the electron cloud results in unrecovered charge, because limited pixel size may result in an error in charge measurement. This is due to the fact that at the silicon K-edge, the charge cloud size suddenly changes. This sudden change, combined with the ASCA x-ray event classification system, results in a disparity at the silicon K-edge.

### **CCD Efficiency**

Efficiency is defined as the fraction of photons which interact in the photosensitive region of the CCD. If the efficiency of the SIS CCD is examined, we see that it varies drastically depending upon the energy of the incoming photon, and that the most apparent characteristics in the efficiency curve are due to the physical nature of the materials which make up the CCD structure and the Lexan and aluminum filter, which is required to prevent any optical light from reaching the CCD.

If efficiency (%) versus photon energy (keV) is plotted, various prominent features can be recognized. [FIGURE 2.2.1] At about 0.5317 keV, a sharp decrease in CCD efficiency identifies the oxygen edge. Photons with this energy are preferentially absorbed in the oxygen found at the CCD surface. This means that these photons are mostly absorbed in the top 1.5  $\mu\text{m}$  of the CCD. Moving on to higher energies, we see a small decrease in efficiency at about 1.5 keV. This identifies the aluminum edge. Photons with this energy are absorbed by the CCD's aluminum filter. The silicon K-edge absorption can be seen at about 1.84 keV. At this point, many photons are stopped in the CCD's gate structure and the efficiency of the CCD is reduced by about 20%. Finally, at high photon energies (greater than about 5 keV) the photosensitive region of the CCD becomes less efficient in detecting the impinging photons.

An experimental determination of CCD efficiency allows us to see that a significant decrease in efficiency will always occur at the silicon K-edge for a semiconductor detector like the SIS CCD. Atomically, what happens at this energy? An x-ray photon with approximately 1.84 keV of energy impinges upon a silicon surface. This photon has just enough energy to knock one of the core silicon electrons out of its shell, but in this process of momentum transfer, the photon itself is "absorbed", leaving a vacancy in the atomic shell. [FIGURE 2.2.2] Therefore, on different sides of the K-edge (as measured on an energy scale), an x-ray photon sees a different interaction depth, i.e., a different mean free path (MFP). Due to the sudden change in the MFP, there is an abrupt change in photon sampling of the photosensitive region, resulting in different charge distributions and thus different amounts of charge diffusion on either side of the K-edge. This is reflected in the CCD efficiency (charge diffusion dynamics will be explained in greater detail in section 2.3).

## ASCA/SIS Grades and Pulseheight Calculations

As the Solid-State Imaging Spectrometer collects data from x-ray sources, many of the energetic photons impinge at the edge of a pixel, rather than in the center. Therefore, charge is distributed between the depletion regions of a few pixels. In order to achieve good energy resolution, all possible x-ray event “splittings” need to be identified and classified so that they can be analyzed. ASCA's on-board computer performs this classification.

When a highly charged pixel is located, the eight surrounding pixels (a 3x3 block) are examined. First, the computer ensures that the central pixel has the highest charge of the nine in the block. Second, the computer checks to see if the pulseheight of this charged pixel is higher than the event threshold of the CCD. If so, it classifies the event and sends the data to earth.

ASCA scientists have established a classification system in which each event can be put into one of seven “grades”. The computer classifies nine pixel events in which the center pixel has the highest charge by comparing each pixel's charge to a set constant called the “split threshold”. Because of the split threshold, we can lose a number of electrons, and this affects the pulseheight calculation. At most, eight times the split threshold can be undetected, if all events are under the split threshold level. If the center pixel is the most highly charged (after the split threshold comparison has been made), the event is classified as S, a single event. If charge is split between the center pixel and a nearest-neighbor pixel (where the neighbor contains at least one split threshold worth of events), the event is P, a single-sided split event. For a situation in which comparable charge is found in the center and two nearest-neighbor pixels forming an “L” shape, the event is appropriately called L, an L-shaped event. Finally, four adjoining pixels with comparable charge are classified as Q, a square-shaped event. There are also a few subsets of each grade. [FIGURE 2.2.3]

Therefore, the SIS CCD disparity is not only affected by ASCA grading, but is also increased by the different classifications of two events near the silicon K-edge whose charge cloud profiles are dissimilar.



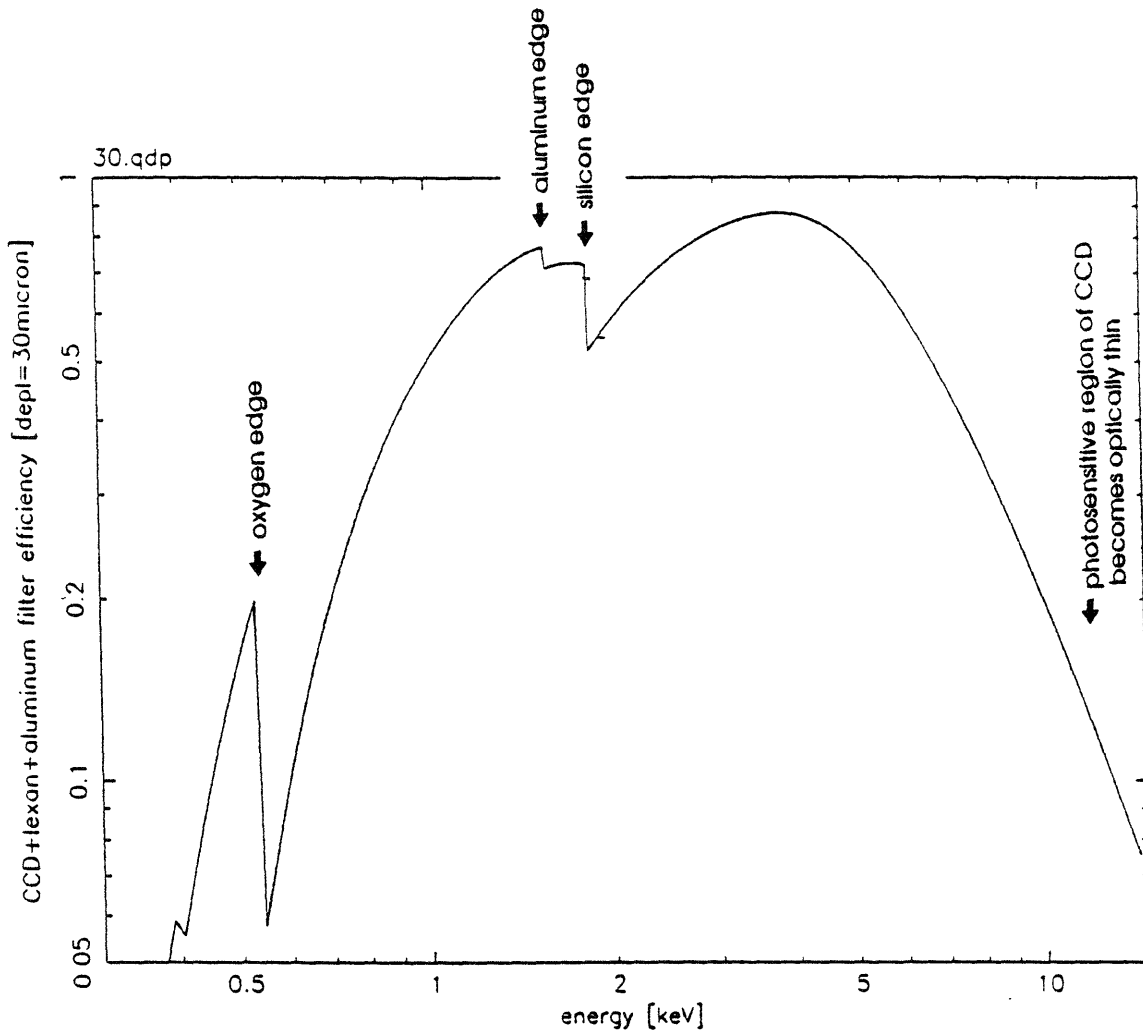
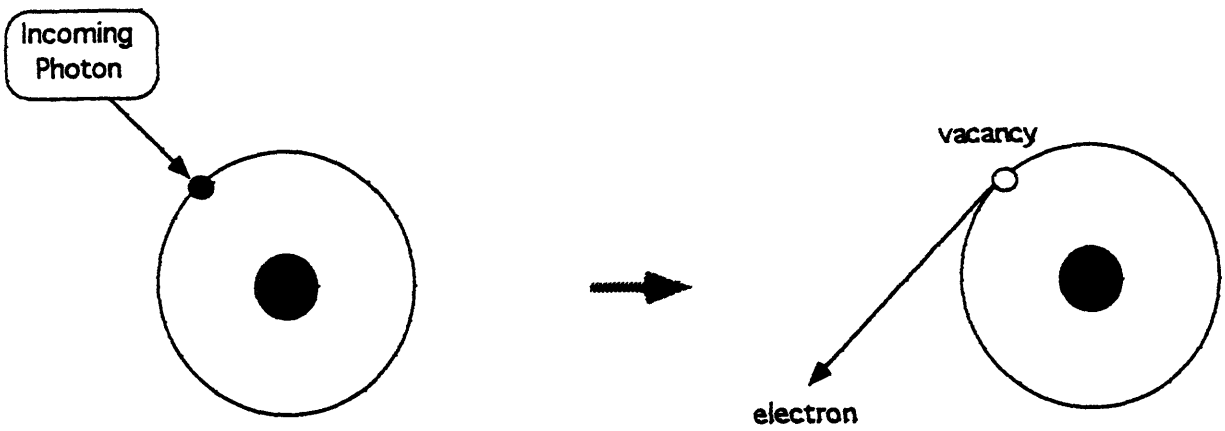
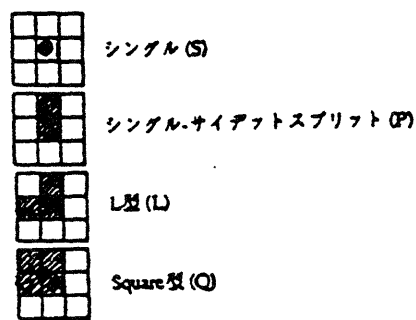


Figure 2.2.1. CCD efficiency (%) vs. Photon energy (eV)



**Figure 2.2.2.** Photoelectric absorption of an x-ray photon.



The four basic types of X-ray event.

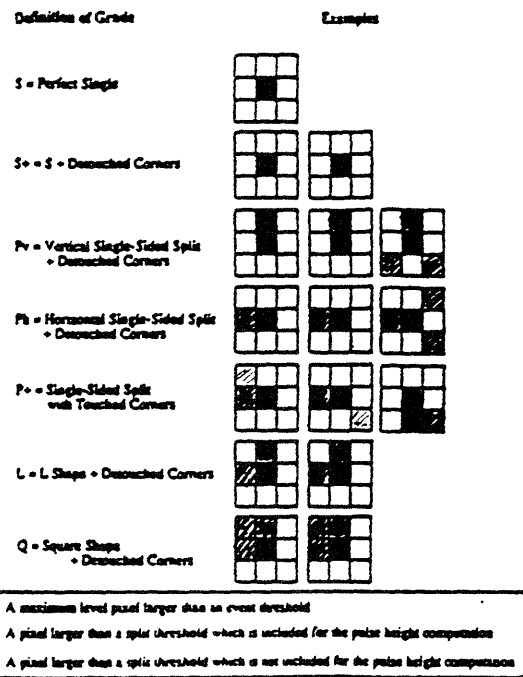


Figure 2.2.3. Various types of ASCA grades. (*Astro-D Technical Description, AO-1 version*)

## 2.3 Theoretical Analysis of X-Ray Induced Charge Cloud

### Diffusion

From CCD performance simulation, at the silicon K-edge, 1.840 keV, we predict a discontinuity in the mean size of the charge cloud at the time of collection,  $\langle\sigma\rangle$ . As the mean charge cloud size within the CCD suddenly changes, charge is lost discontinuously, and we see a disparity between charge deposited on the CCD surface and output pulseheight.

How is charge “lost discontinuously”? This loss occurs because the mean free path of photons as they enter the CCD is drastically different for photon energies above and below the K-edge energy. For energies slightly below the K-edge, the mean free path discontinuously increases. Thus, the charge cloud size also increases. This greater diffusion, coupled with the fact that pixel size in the CCD is limited, causes some charge to be lost in the charge collection.

This diffusion profile can be understood by theoretical modeling. Modeling is useful in order to be able to predict results from actual SIS data. Through modeling, CCD behavior was analyzed by studying the expected amount of deviation in the CCD charge output at the silicon K-edge. This theoretical analysis was done by comparison of the size of induced electron clouds whose “source” x-rays have energies on either side of the silicon K-Edge. This allows us to see the predicted difference in this diameter at the two different energy ranges.

In order to study the spatial extent of the x-ray induced charge cloud in silicon, we must first look at its dynamics. An initial assumption which must be made is that the charge distribution,  $q(x,y)$ , within the CCD is of Gaussian form:

$$q(x,y) = \frac{Q}{2\pi\sigma^2} \exp\left[-\frac{(x-x_0)^2 + (y-y_0)^2}{2\sigma^2}\right]$$

where  $x, y$  are the spatial coordinates of the CCD surface,  $x_0, y_0$  refer to the center of the distribution,  $\sigma$  is the width of the distribution, and  $Q$  is the original charge of the charge cloud produced by the incoming x-ray.

Using this assumption and the diffusion equation, we can make some conclusions about the initial size and change in size of the charge cloud. The diffusion equation states that

$$\frac{\partial n}{\partial t} = D \nabla^2 n$$

where  $n$  is the concentration of charged particles (number per unit volume), and  $D$  is the carrier diffusion constant in silicon.

The initial condition that we are supposing is that at the time of the x-ray photon impact, all events in the cloud are modeled as a Gaussian at the originating impact point. Therefore,  $n(x,y,t)$ , the shape of the Gaussian at a subsequent time,  $t$ , is of the form

$$n(x,y,t) \propto \exp\left\{-\left[\frac{(x-x_0)^2}{4Dt} + \frac{(y-y_0)^2}{4Dt}\right]\right\}$$

which gives the result that

$$2\sigma^2 \approx 4Dt$$

or

$$\sigma \approx \sqrt{2Dt}$$

In other words, we can say that the size of the charge cloud within the CCD is a function of the diffusion constant of the material and the time elapsed.

Now, in order to find  $\langle \sigma \rangle$ , the average charge cloud size, we need to find the drift time of the charge cloud, or the time it takes to drift from the interaction point at depth  $x_I$  to the junction depth  $x_J$ :

$$t(x_I) = \int_{x_I}^{x_J} \frac{dx}{-\mu_e E(x)}$$

Here  $\mu_e$  is the electron mobility in p-type silicon, and  $E(x)$  is the electric field at depth  $x$ . Following the derivation in Bautz (Astro-D Memo #465), we get the final result:

$$t(x_I) = \epsilon_s \epsilon_0 \rho \frac{\mu_h}{\mu_e} \ln \left\{ \frac{x_D - x_J}{x_D - x_I} \right\}$$

$$t(x_I) = (2.25 \text{ ns}) \cdot \left( \frac{\rho}{6500 \text{ } \Omega \cdot \text{cm}} \right) \cdot \ln \left( \frac{x_D - x_J}{x_D - x_I} \right)$$

where  $\epsilon_s$  is the relative permittivity of silicon,  $\epsilon_0$  is the relative permittivity of free space,  $\rho$  is the average resistivity of silicon in the depletion region,  $x_J$  is the junction depth,  $x_D$  is the depletion region depth ( $\approx 35 \mu\text{m}$ ), and  $x_I$  is the depth of the point of interaction of the x-ray.

The broadening of the charge cloud can be found from the following equation:

$$\sigma_{\text{Individual Photon}}^2 = \sigma_I^2 + \sigma_{\text{drift}}^2(x_I)$$

or

$$\sigma^2(x_I) = \frac{D_i^2}{20} + 2D_n t(x_I)$$

where  $D_i$  is the initial charge cloud diameter (which is multiplied by a factor of 1/20 due to a geometric assumption), and  $D_n$  is the minority carrier diffusion coefficient in the depletion region of the CCD. The initial size of the charge cloud is about  $2\sigma$ , or

$$2\sigma \approx 0.017[E \text{ (keV)}]^{1.75} \mu\text{m}$$

Noting that

$$\sigma \approx \sqrt{2Dx}$$

we get

$$\sigma^2(x_I) = \frac{D_i^2}{20} + \sigma_D^2 \cdot \ln\left[\frac{x_D - x_I}{x_D - x_I}\right]$$

where  $\sigma_D \approx 3.5 \mu\text{m}$ .

Now we would like to find the theoretical mean charge cloud size in silicon as a function of energy. By doing this, we will be able to theoretically study the mean interaction depth of the x-rays at energies on both sides of the K-edge. The mean sigma can be found by integrating  $\sigma(x_I)$  over all interaction distributions.

$$\langle \sigma \rangle = \frac{\int N(x_I) \sigma(x_I) dx_I}{\int N(x_I) dx_I}$$

$N(x_I)$  is the interaction distribution in the CCD structure:

$$N(x) = \mu(E) \cdot \exp[-\mu(E) \cdot x]$$

$\mu(E)$  being the linear absorption coefficient for silicon.

$$\mu(E) = \frac{\alpha}{\eta(\text{Si})} = \frac{2\lambda r_o f_2}{\eta(\text{Si})} \text{ [cm}^{-1}\text{]}$$

Here  $\alpha$  is the atomic photoabsorption cross-section, which is a function of  $\lambda$ , wavelength,  $r_o$ , the classical electron radius, and  $f_2$ , the X-Ray Scattering factor. Note that  $\alpha$  is the quantity which changes drastically at the K-edge.

$\eta(\text{Si})$  is defined to be

$$\eta = \frac{A}{N_o \cdot \rho(\text{Si})}$$

where  $A$  is the atomic weight,  $N_o$  is Avogadro's number, and  $\rho$  is the density of silicon.

Using these definitions we find that

$$\begin{aligned} \langle \sigma \rangle &= \int_0^{\infty} N(x_I) \sigma(x_I) dx_I \\ &= \int_0^{\infty} \left[ \frac{(0.017)^2 (E)^{3.5}}{20} + (3.5)^2 \ln\left(\frac{x_D - x_I}{x_D - x_I}\right) \right]^{\frac{1}{2}} \cdot \mu(E) \cdot \exp(-\mu(E) \cdot x_I) dx_I \end{aligned}$$

This is the final integral which must be solved for energies above and below the K-edge. In the simulator program mentioned previously, this integral is calculated by random sampling and rejection, giving a mean sigma profile with a small discontinuity.

In order to practically compute the solution to this integral, we need to make some strong assumptions. We know that the amount of charge collected in the central pixel (for single events) is a function of three spatial variables,  $x$ ,  $y$ , and  $z$  ( $z$  refers to the interaction



depth of the photon). In order to estimate the disparity between charge collected by the CCD and output pulseheight at the silicon K-edge, we first contract the z-dependence of the above integral and then average over x and y to get the mean collected charge. If we evaluate this function of mean collected charge, the sudden change in the range of the x-ray photon impinging on the CCD (looking across the K-edge) will give us two different “charge-cloud” profiles. These two different profiles will result in a change in the fractional “area” of the pixel which produces single events. The change can also be seen as a difference in the average fractional charge collected by the CCD, which is the disparity for which we are searching.

The amount of charge collected in the central pixel for single events as a function of x and y within the pixel can be approximated as a Gaussian function. If we take an arbitrary originating point for the charge cloud, this function can be written as:

$$f(x, y | x_0, y_0) = \frac{1}{2\pi \langle \sigma \rangle^2} \exp\left[-\frac{(x-x_0)^2 + (y-y_0)^2}{2\langle \sigma \rangle^2}\right]$$

Now, we want to find an “allowable region” of  $(x_0, y_0)$  so that almost all the charge lies in the center pixel. That is, we want a situation in which less than forty electrons (the split threshold) fall into a single neighboring pixel. In order to do this we must average the fractional charge over the pixel face.

$$q(x_0, y_0) = \int_{-\frac{\text{pixel}}{2}}^{\frac{\text{pixel}}{2}} dx \int_{-\frac{\text{pixel}}{2}}^{\frac{\text{pixel}}{2}} dy \frac{1}{2\pi \langle \sigma \rangle^2} \exp\left[-\frac{(x-x_0)^2 + (y-y_0)^2}{2\langle \sigma \rangle^2}\right]$$

The limits of  $q$  are relatively straightforward: for  $(x_0, y_0) = (0, 0)$ ,  $q$  is approximately equal to the original incoming charge  $Q$ . For  $x_0 = \pm (\text{pixel}/2)$  and  $y_0 = \pm (\text{pixel}/2)$ ,  $q$  is approximately  $Q/4$ .

In the general case, we can use separation of variables in order to solve the integral.

$$q(x_0, y_0) = \int_{-\frac{\text{pixel}}{2}}^{\frac{\text{pixel}}{2}} \frac{1}{\sqrt{2\pi} \langle \sigma \rangle} \exp\left[-\frac{(x-x_0)^2}{2\langle \sigma \rangle^2}\right] dx \int_{-\frac{\text{pixel}}{2}}^{\frac{\text{pixel}}{2}} \frac{1}{\sqrt{2\pi} \langle \sigma \rangle} \exp\left[-\frac{(y-y_0)^2}{2\langle \sigma \rangle^2}\right] dy$$

Solving for the  $x$ -variable and making a change of variables, we get

$$q(x_0) = \frac{\sqrt{2} \langle \sigma \rangle}{\sqrt{2\pi} \langle \sigma \rangle} \int_{\frac{\frac{\text{pix}}{2} - x_0}{\sqrt{2} \langle \sigma \rangle}}^{\frac{\frac{\text{pix}}{2} + x_0}{\sqrt{2} \langle \sigma \rangle}} \exp(-t^2) dt \quad \text{where } t = \frac{x - x_0}{\sqrt{2} \langle \sigma \rangle}, \quad dt = dx \frac{1}{\sqrt{2} \langle \sigma \rangle}$$

Solving this equation gives a function consisting of two similar erf functions, whose arguments only differ by a sign:

$$q(x_0) = \frac{1}{\sqrt{\pi}} \left[ \text{erf}\left(\frac{\text{pix}}{2\sqrt{2} \langle \sigma \rangle} - \frac{x_0}{\sqrt{2} \langle \sigma \rangle}\right) - \text{erf}\left(-\frac{\text{pix}}{2\sqrt{2} \langle \sigma \rangle} - \frac{x_0}{\sqrt{2} \langle \sigma \rangle}\right) \right]$$

Therefore, the total solution to the integral is

$$q(x_0, y_0) = \frac{1}{\pi} \left[ \text{erf}\left(\frac{\text{pix}}{2\sqrt{2} \langle \sigma \rangle} - \frac{x_0}{\sqrt{2} \langle \sigma \rangle}\right) - \text{erf}\left(-\frac{\text{pix}}{2\sqrt{2} \langle \sigma \rangle} - \frac{x_0}{\sqrt{2} \langle \sigma \rangle}\right) \right] \\ \cdot \left[ \text{erf}\left(\frac{\text{pix}}{2\sqrt{2} \langle \sigma \rangle} - \frac{y_0}{\sqrt{2} \langle \sigma \rangle}\right) - \text{erf}\left(-\frac{\text{pix}}{2\sqrt{2} \langle \sigma \rangle} - \frac{y_0}{\sqrt{2} \langle \sigma \rangle}\right) \right]$$

Here we can see that the fractional charge,  $q$ , is a two-dimensional surface function. Its peak is at  $(x_0, y_0) = (0,0)$  and it falls off gradually as  $|x|$  and  $|y|$  approach  $(\text{pixel}/2)$ .

In order to see the CCD non-linearity, we calculate the mean height at the central part of this function for energies above and below the silicon K-edge. Interpretation of this function results in the observation of the expected disparity in the value of  $\langle\sigma\rangle$  for values greater than and less than that of the silicon K-edge;  $\langle\sigma\rangle$  is fairly consistent for energies less than that of the edge, but as x-ray energies increase past the K-edge, it is suddenly reduced. The theoretical disparity found in this manner is on the order of 1-2%.

The change in the mean charge cloud size can be interpreted as a result of a change in the mean free path of x-rays in silicon at various energies. When the mean free path changes as energies “cross” the K-edge, the mean interaction depth of the x-ray changes. Thus the size of the charge cloud created by photon interactions also changes, because a different interaction depth means a longer drift time, ultimately resulting in a larger charge cloud. [FIGURE 2.3.1]

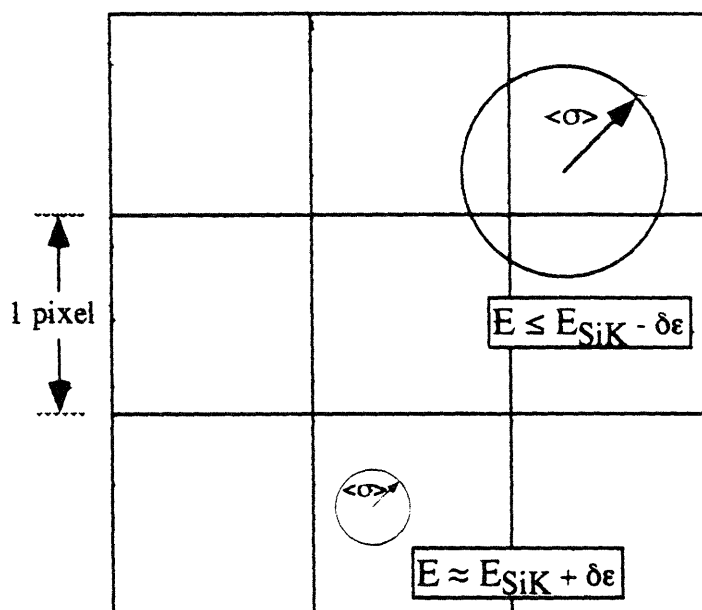


Figure 2.3.1. Comparison of charge cloud sizes for different input energies.

## **Chapter 3**

# **Investigation of Energetic Interactions Within the SIS**

The next step in the investigation into the behavior of the SIS CCDs is the analysis of actual SIS data. The theoretical discontinuity found in the previous section should be apparent in data taken from the SIS CCDs. In order to find and quantify the actual value of the discontinuity, I analyzed data already acquired from the SIS in order to model the CCD. Specifically, in order to see the small variation in CCD output, I studied CCD data generated by a High Resolution Erect Field (HIREFS) spectrometer. The HIREFS is a grazing incidence diffraction grating spectrometer used to calibrate the SIS.

### **3.1 The Spectrometer and the Dispersion Solution**

For this study, I have concentrated on the analysis of six large data sets. The main characteristics of the data I used are summarized in Table 3.1.

**Table 3.1.1. Characteristics of Data Used in Final Analysis**

<b>Parameter</b>	<b>Definition</b>	<b>Value</b>
CCD	Particular chip used	chip 1, sensor 3
Neat Number	Position of linear stage of CCD mount	5500
Scan Number	Position of spectrometer grating	3100
Spectral Order	Order of energy spectrum, in range of K-edge energy	3
Grade	Type of grading of photon events used	Single events, Grade 0
Number of Events	Number of photons in data set analyzed	≈ 16800

In the general case, the function of a spectrometer is to “decompose” an incoming electromagnetic wave into its spectral components. The HIREFS separates the incoming x-rays by use of a reflection diffraction grating. X-rays of different wavelengths, impinging upon the grating, are reflected in different directions. In this way, the grating produces an x-ray spectrum. In most cases, the reflection grating will produce more than one spectrum. “First order” refers to the two spectra on either side of the axis/origin point (determined by the spectrometer set-up). The next two spectra are called “Second order”, etc.

There is a basic relationship between wavelength of incoming x-ray and the angle at which the spectral component of the x-ray will be reflected off of the diffraction grating. This relationship is called the grating equation:

$$n\lambda = d \cdot \sin\Theta$$

Here, n is a whole number, d is the distance between grooves on the diffraction grating,  $\lambda$  is the wavelength of the impinging x-ray, and  $\Theta$  is the resultant angle “displacement”.

In the HIREFS spectrometer, the x-ray spectra are recorded on the SIS CCD. By looking at the CCD output, we can search for characteristic behavior within the silicon of the device. [FIGURE 3.1.1]

The initial step in using the HIREFS data is understanding the dispersion of this spectrometer. To do this, we must analyze the specific grating equation of the spectrometer and then find a relationship between the wavelength of the incoming x-ray and the spatial position on the resultant x-ray spectrum for the HIREFS. This general relationship is called the “dispersion solution” of the spectrometer. Careful study of the dispersion relation will allow the measurement of energy deviations in the CCD output to be done in a very precise manner.

If we first look at the spectrometer set-up, we see that the main component of the spectrometer is the diffraction grating which separates incoming electromagnetic energy into multiple orders. [FIGURE 3.1.2]

The grating equation derived from this set-up (which is given in the spectrometer specifications) relates the y variable, a relative linear coordinate, to the order times the known absolute wavelength of a spectral line, given the scan number, and neat number of the data, and also the parameters L,  $y_0$ , and  $\sigma_0$  (the groove spacing at the grating center):

$$\lambda = (\sin \beta - \sin \alpha) \cdot \frac{\sigma_0}{m}$$

$$\text{where } \beta = 2\Theta - \alpha + \tan^{-1} \left[ \frac{y + \text{OFFSET}}{L} \right]$$

Simplifying these known equations into a single equation gives the form of the dispersion solution for which we are searching:

$$\lambda(y) = \left\{ \sin \left[ 2\Theta - \alpha + \tan^{-1} \left( \frac{y + \text{OFFSET}}{L} \right) \right] - \sin \alpha \right\} \cdot \frac{\sigma_o}{m}$$

This relationship between y-coordinate on the CCD frame and wavelength of x-rays can be used to translate the CCD frame “picture” into an energy profile of the x-rays, and subsequently can be used to find the relation between incoming energy and pulseheight output by the CCD.

In order to reach our goal of quantifying the dispersion solution and being able to model and constrain spectrometer operations, we must first consider two important issues: spectrometer resolution and CCD gain.

The resolution of the spectrometer is an important characteristic to note for the simple reason that in our study, the search for a disparity between input and output CCD energy depends strongly upon the resolution of the CCD. If CCD resolution is relatively poor, the disparity will not be found, and therefore will be unimportant in the quantification of CCD behavior. However, if the spectrometer resolution is poor, observation of the disparity will be impossible. A study of HIREFS specifications shows that the spectrometer has a much higher degree of resolution than the CCD. This fact ensures that variations in output that we see in our results stem from errors in the CCD's resolution, not the spectrometer's. Therefore, the disparity, if significant, should be visible in the data analysis.

Another important characteristic which must be studied is the CCD gain, or, in other words, the relationship between incident x-ray energy and output signal from the detector. In order to find this relationship, we must look at one representative set of CCD data, and determine the nearly linear correspondence between the expected x-ray spectral line energies and the recorded CCD pulseheight.



Taking the cumulative set of CCD data, we plot pulseheight versus y-coordinate for all the data points. This results in a spread of spectral orders within which we can see strong peaks. [FIGURE 3.1.3] These peaks are associated with known characteristic x-ray line energies. Finding the gain of the system consists of finding the relationship between the pulseheight (in ADU, analog to digital units) of the few strongest peaks and their known energies (in electron-volts). In my particular case, I used four prominent peaks for my gain calculation:

<u>Line</u>	<u>Pulseheight (ADU)</u>	<u>Energy (eV)</u>	<u>Gain (eV/ADU)</u>
Oxygen	169.8	524.9	3.0913
Magnesium	410.2	1253.6	3.0561
Tungsten	447.5	1383.5	3.0916
Tungsten	577.4	1775.4	3.0748

In order to find the gain (in a first approximation), we linearly fit the above data:

$$\text{Energy} = \alpha \cdot \text{ADU} + \beta$$

The linear fit gives an intercept consistent with the model of a line through the origin (i.e.  $\beta=0$ ). Therefore, as a first approximation to the gain, we can take the average of the gains found above to find  $\alpha$ , the relationship between energy and ADU. This gives an average gain of 3.0785 eV/ADU, which is what we take to be the approximate relationship between eV and ADU in this system.

Once we find the theoretical form of the dispersion solution and the gain of the CCD system, we can go about finding the actual dispersion solution. We do this by fitting the CCD data to the form of the dispersion solution. I chose to go about doing this in the following way. Taking the original cumulative CCD frame of data, I once again plotted a

view of pulseheight as a function of  $y$  (the spectral orders). I then identified eight lines, or peaks on this plot and recorded the pulseheight and order of each:

<u>Order</u>	<u>Pulseheight (ADU)</u>	<u>y value (<math>\pm 2.5</math> pixels)</u>
1	169.8	145
2	410.2	270
2	450.8	325
3	447.5	47
3	577.4	227
3	595.7	247
4	577.4	20
4	596.6	45

I determined the pulseheight of each peak by plotting a histogram of number of events as a function of pulseheight and then fitting my results with a Gaussian curve. The  $y$  value was approximated and therefore has been given an appropriate constant error estimate.

The identification of these eight peaks gave me enough data to find a fit for the dispersion solution. In order to fit while accounting for errors in the  $y$ -direction, the dispersion solution was inverted to get  $y$  as a function of wavelength:

$$y(\lambda) = L \cdot \tan \left[ \sin^{-1} \left( \frac{m}{\sigma_0} \lambda + \sin \alpha \right) - 2\Theta + \alpha \right] - \text{OFFSET}$$

For even more ease of calculation, wavelength was converted to energy:

$$y(E) = L \cdot \tan \left[ \sin^{-1} \left( \frac{m}{\sigma_0} \cdot \frac{hc}{E} + \sin \alpha \right) - 2\Theta + \alpha \right] - \text{OFFSET}$$

(here  $h$  is Planck's constant, and  $c$  is the speed of light). I then fit for four parameters:  $\alpha$ ,  $-(\sigma_0/m)^{-1}$ ,  $L$ , and the offset ( $2\Theta$  was given to be 3.077179). Through the method of

minimization of the chi-squared parameter, I determined that the results from the fit were as follows:  $\alpha = 1.550$  radian,  $(\sigma_0/m)^{-1} = 3.3907 \times 10^{-5} \text{ \AA}^{-1}$ ,  $L = 4.0139 \times 10^4$  pixels, and offset = 28.26 pixels. [FIGURE 3.1.4]

As stated previously, in order to determine the accuracy of this fit, I looked at the weighted variance, or chi-squared parameter. Chi-squared is a statistic which characterizes the dispersion of the observed data from the expected data. It is defined as:

$$\chi^2 \equiv \sum_{\text{all points}} \frac{(\text{data} - \text{model})^2}{\sigma_{\text{data}}^2}$$

where  $\sigma$  is the standard deviation of the data. Here, the numerator measures the discrepancy between the model and the data, while the denominator measures the expected uncertainty of the data. For good agreement in the results, the discrepancy should correspond to the expected error, and chi-squared should go as the number of degrees of freedom of the data. For this fit, the value for chi-squared was 5.972.

Usually the reduced chi-squared is used to judge the accuracy of the fit. Reduced chi-squared is defined to be

$$\text{Reduced } \chi^2 = \frac{\chi^2}{\# \text{ of points} - \# \text{ model parameters}}$$

where the number of degrees of freedom correspond to the number of variable parameters in the curve fit. The expectation value of the reduced chi-squared parameter is 1, meaning that if the result we get is close to 1, we have a good fit. If the reduced chi-squared is large, this means that large deviations from the assumed distribution exist; if it is small, this may imply that errors have been overestimated or the problem is under-constrained. The reduced

chi-squared we get in this case is 1.493. Since we have a small number of points in our fit, this reduced chi-squared value implies that this is consistent with a good fit to the data.

Therefore, the final dispersion solution we find is

$$y(E) = 40139 \cdot \tan \left[ \sin^{-1} \left( -3.3907 \times 10^{-5} \cdot \frac{hc}{E} + \sin [1.550] \right) - 2\Theta + 1.550 \right] - 28.26$$

or

$$E(y) = \frac{(-0.42039)}{\left\{ \sin [1.5218 + \tan^{-1} \left( \frac{y + 28.260}{4.0139 \times 10^4} \right)] - 0.99978 \right\}}$$

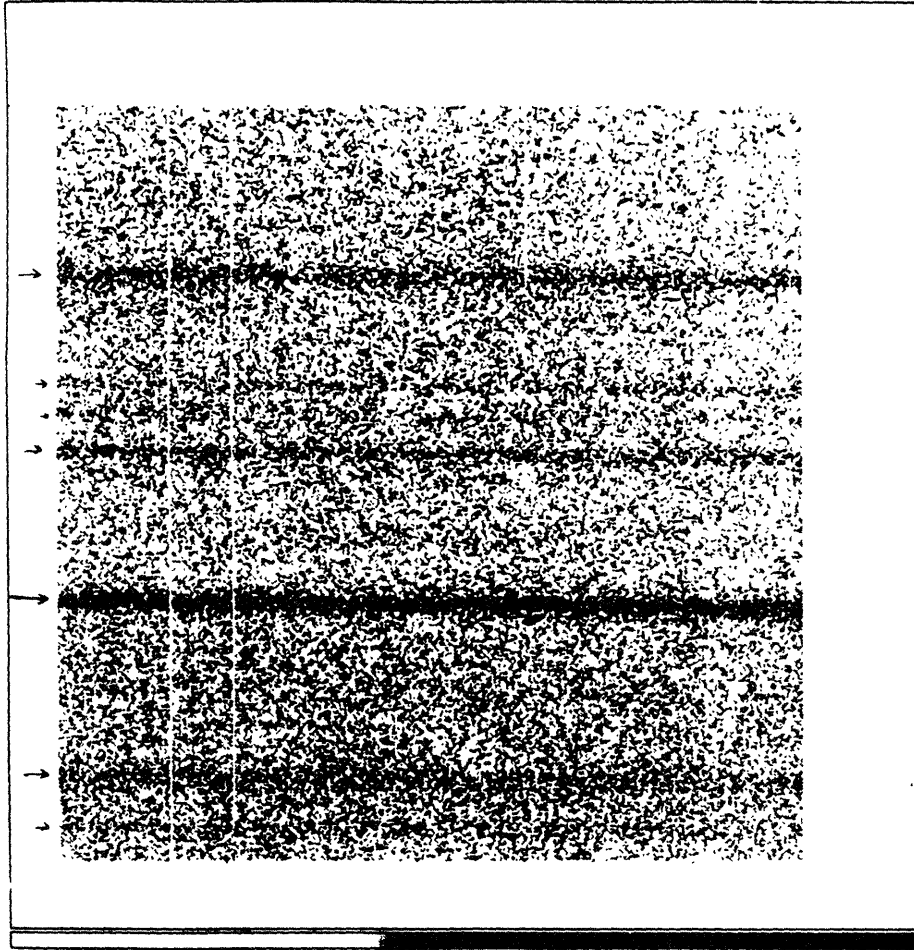


**Figure 3.1.1.** Typical CCD frame of data.



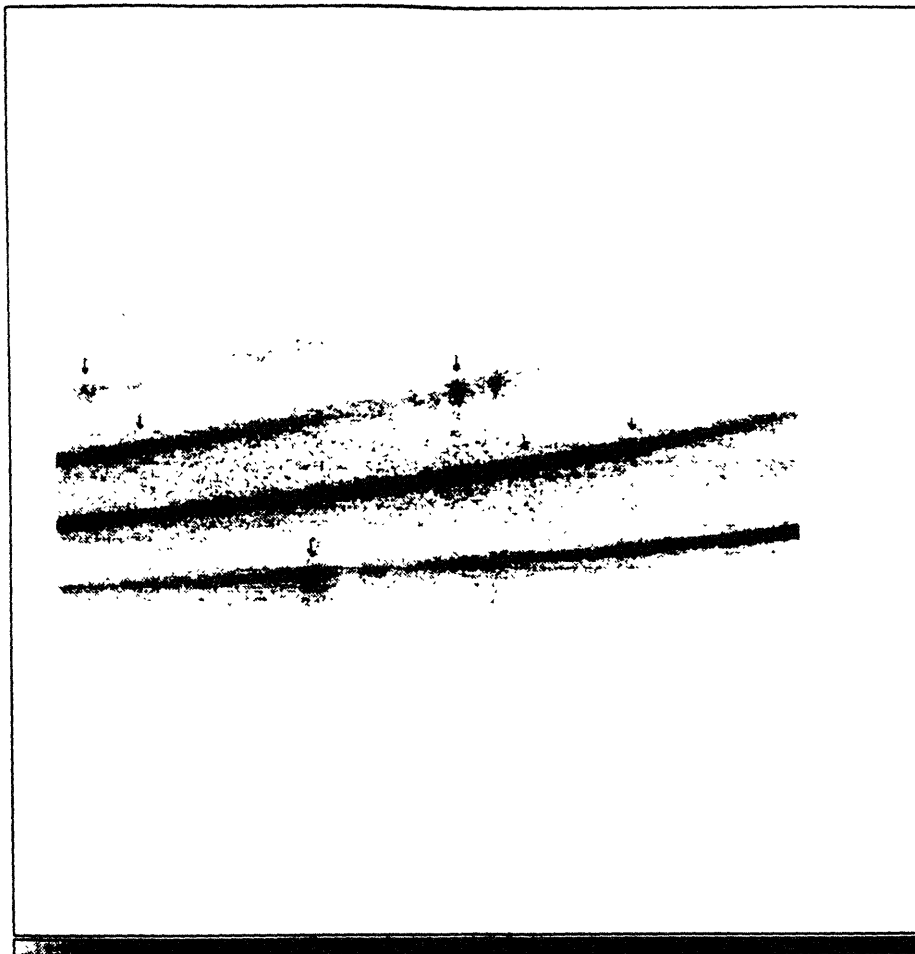


**Figure 3.1.3.** Output pulseheight vs. y coordinate, noting a few spectral "lines" or peaks.

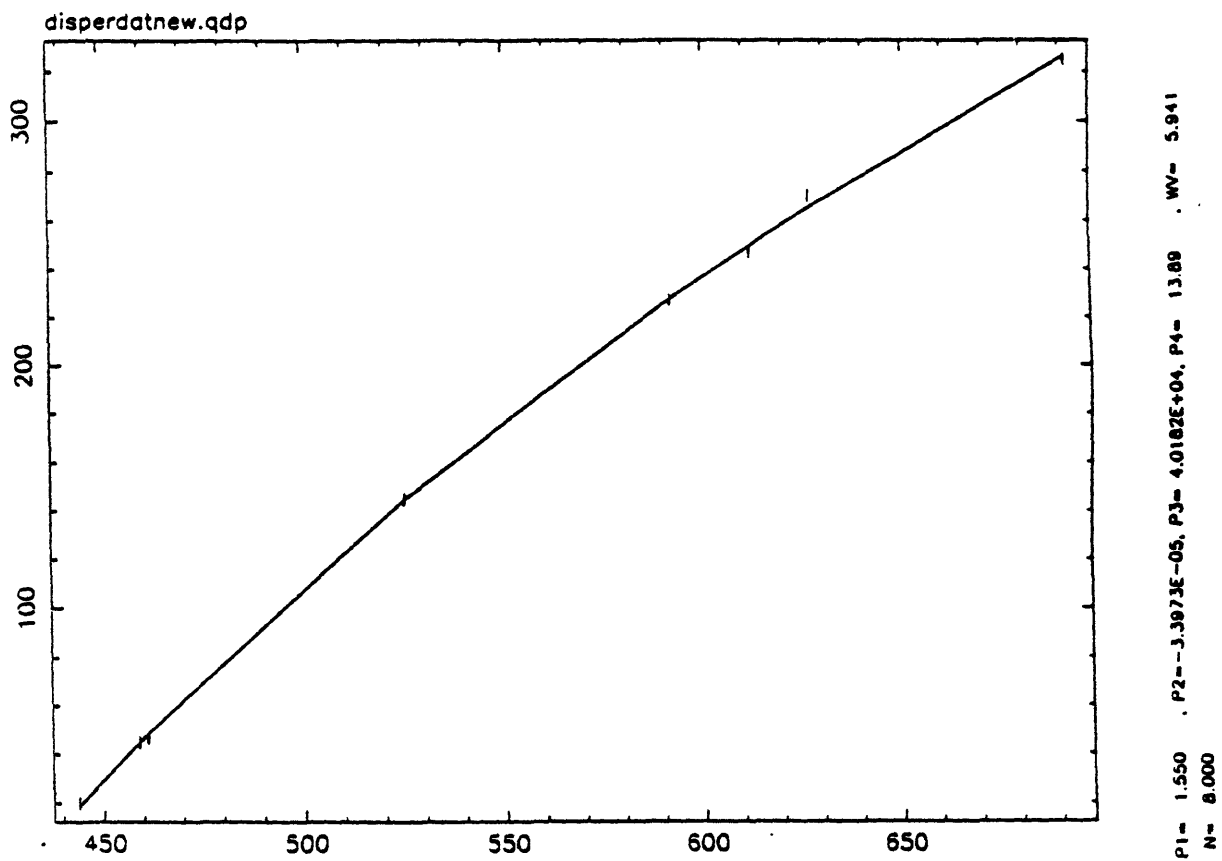


**Figure 3.1.4.** Fitting the data in order to determine the dispersion solution of the spectrometer.



## 3.2 SIS CCD Analysis

### CCD Frame Rotation

Before performing a final analysis of CCD characteristics, an important factor to consider is the possible existence of a small CCD frame rotation relative to the spectrometer. In other words, the actual CCD frame may have been at a small rotated position when data was being recorded. Accounting for this rotation angle is important, because it may influence the precision of the pulseheight analysis.

In order to determine the amount of rotation in the data being used in this investigation, selected strong lines were filtered out of the original frame of CCD data.

The slope of these strong lines was measured to be approximately  $-4.4 \times 10^{-3}$ . Thus the angle of rotation of the data frame was determined to be

$$\begin{aligned}\Theta &= \tan^{-1}(-4.4 \times 10^{-3}) \\ &= -0.252^\circ\end{aligned}$$

Using this angle of rotation, I was able to estimate the amount by which energy peak measurements have been “smeared out”.

By how much does the rotation confuse energies? An angle of  $\approx -0.252^\circ$  over a distance of approximately 425 pixels results in a “blurring effect” of

$$\Delta_{\text{error}} = \# \text{ of pixels} \cdot \tan(\Theta_{\text{rot}})$$

$$\Delta_{\text{error}} \approx 1.87 \text{ pixels}$$

This blurring effect ultimately causes an error of  $\Delta_{\text{error}}/2$  in the measurement of an energy peak. This energy peak error is

$$\Delta_{\text{error}}/2 \approx 0.935 \text{ pixels}$$

Using the dispersion solution found earlier, this error in pixels corresponds to an error of approximately 0.43 eV.

Neglecting this peak measurement error will result in a small error in the dispersion solution. Is this error significant in this study? Table 3.2 summarizes how this error compares to the other existing errors which appear in the energy measurements.

**Table 3.2.1.** Accounting for Errors in Energy Measurement (for Oxygen line, 524.9 eV).

Type of Error	Description	Amount of Error
$\Delta y$	Constant @ 524.9 eV	0.3412 pixels
$\Delta E/\Delta y$	eV/pixel @ 524.9 eV	0.4320 eV/pixel
$\Delta E$	Spectrometer's intrinsic resolution	0.1474 eV
$(\Delta E/E)_{\text{CCD}}$	Energy measurement error from CCD @ 524.9 eV	0.0503
$(\Delta E/E)_{\text{rotation}}$	Energy measurement error due to frame rotation @ 524.9 eV	$8.192 \times 10^{-4}$ for 425 pixels in x
$(\Delta E/E)_{\text{TOT}}$	Maximum possible error, accounting for above	0.0503

Since the error due to frame rotation is quite small, I determined that the rotation angle of the data was too small to be of significance in this study. I therefore did not take it into consideration in my final analysis.

## Final Analysis

At this point, the final analysis was performed. Once the dispersion solution was determined, the next step was to search for the non-linearity in the Energy/Pulseheight relation. One effective method for searching for this small (1-2%) disparity is to plot the percentage difference between incident energy and resultant pulseheight for all incoming energy values. In my particular case, I plotted  $\Delta E$  vs.  $y$ , where

$$\Delta E = \frac{\text{Expected Energy} - \text{Pulseheight}}{\text{Expected Energy}}$$

Here I selected to plot as a function of the  $y$  value, rather than the related  $E$  value, so that my data would be distributed evenly over a wider range.

In theory, a plot of  $\Delta E$  vs.  $y$  should give results close to zero for almost all values; however, as we approach the silicon K-edge, there should be a gradually increasing upwards peak which sharply decreases right at the silicon-K edge. [FIGURE 3.2.1]

The disparity should also be present in a plot of the actual data. According to the dispersion solution found earlier, in  $y$ -units the silicon K-edge would lie at  $y = 230$ .

For simplicity, I decided to plot only single events in my search for the non-linearity. I began with a basic straightforward plot of  $\Delta E$  vs.  $y$ . When I plotted this data I found a large amount of variance in the data points; however, this plot did allow me to verify that my dispersion solution was adequate, because the zero crossings of this plot occur at appropriate  $y$  values [FIGURE 3.2.2] This first result prompted many varied levels of fine-tuning of the data.

Since many data points existed for each  $y$  value, I decided to average the set of  $\Delta E$  values for each  $y$  value. This method would not only minimize noise, but it would also allow me to get one mean  $\Delta E$  corresponding to each  $y$ . In addition to finding the mean of each single bin of  $\Delta E$  values, I calculated the uncertainty in the mean by finding the standard deviation of the mean, which is a measure of uncertainty due to fluctuations in

data observations which we find in our attempt to determine the “true” value of the data. The standard deviation of the mean is found from the standard deviation:

$$\text{Standard Deviation} = \sigma = \sqrt{\lim_{N \rightarrow \infty} \left[ \frac{1}{N} \sum_i x_i^2 \right] - \mu^2}$$

$$\text{Standard Deviation of the Mean} = \sigma_\mu = \frac{\sigma}{\sqrt{N}}$$

Here, the  $x_i$  are the data points,  $\mu$  is the mean of the data, and  $N$  is the number of data points in the sample. (See Appendix D for my averaging programs.)

Determination and subsequent plotting of the averaged  $\Delta E$  values and their uncertainties resulted in a plot with much less noise than the previous one; however, a substantial amount of variance was still present in the data, especially at higher energy values, where less events went into each data point. In order to limit the variance to an even greater extent, I combined the data from three sets (or chops) and averaged  $\Delta E$  for each  $y$  value for the cumulative set. Again, I found a result with lower noise, but the disparity was still not visible. [FIGURE 3.2.3]

In order to reduce variation in the data still further, I moved on to averaging  $\Delta E$  values for every five [FIGURE 3.2.4] and then every ten  $y$  values [FIGURE 3.2.5]. This method allowed me to greatly reduce noise; however, uncertainty in the data still masked the appearance of any disparity.

At this point, further options for basic averaging seemed limited. I then followed another approach in the data analysis. I began by histogramming bins of  $\Delta E$  values for every ten  $y$  units. I then fit the resulting histograms with a gaussian curve in order to find, first, a central  $\Delta E$  value for each, and second, an uncertainty (or error bar) with a range within which the reduced chi-squared value would increase by one. These results were

also plotted, but once again, problems with noise in the data gave an inconclusive picture.

[FIGURE 3.2.6]

An important observation we must consider here is that in analyzing the averaged data plots, we notice that there seems to be a constant offset in the  $\Delta E$  calculation; for an accurate fit of the data to the dispersion solution, the averaged values should be, on average, at  $\Delta E$  equals zero. How can we account for the difference from zero? The most likely reason for this error is that our previous calculation of CCD gain, which was based on only a few spectral lines, is in error. This systematic error would cause a constant error in the  $\Delta E$  calculation, which would manifest itself as a constant offset in our averaged-data plots (systematic errors such as this will be discussed further in the next section).

Since the above analysis methods were not conclusive, I then attempted to look for the disparity by narrowing my search to look for any variation in the region of the silicon K-edge. I approached this analysis in two ways. First, I modeled the data as a linear curve with a discontinuity at the silicon K-edge ( $y= 230$  ADU). Following this reasoning, I hypothesized that the average value for  $\Delta E$  below the silicon K-edge, averaged over all data points, would be lower than the average value for  $\Delta E$  for points just above the K-edge. I calculated these averages first for  $y$  values ranging from 180 to 220 ADU, and then for 240 to 310 ADU. My results were

$$\langle \Delta E \rangle_{\text{low}} = 0.0070$$

$$\langle \Delta E \rangle_{\text{high}} = 0.0076$$

These values are not consistent with the disparity for which we are searching; they demonstrate that the disparity may be masked because of the amount of variance which exists in the data (primarily in the data corresponding to values above the K-edge).

The second approach I took in my more focused data analysis followed from the first. In this approach, I fit my averaged data with two separate lines: one below the K-

edge, and one above the K-edge. In doing this I hoped to find a positive-sloped linear fit to  $\Delta E$  below the edge, and a different linear fit to the data above the edge. My results were as follows:

Linear curve fit to data below Si K-edge: ( $180 < y < 220$  ADU)

$$\Delta E \approx (-1.90 \times 10^{-5} \pm 1.72 \times 10^{-4})y + (1.08 \times 10^{-2} + 3.44 \times 10^{-2})$$

Linear curve fit to data above Si K-edge: ( $240 < y < 310$  ADU)

$$\Delta E \approx (1.28 \times 10^{-4} \pm 1.79 \times 10^{-4})y + (-2.76 \times 10^{-2} \pm 4.93 \times 10^{-2})$$

As we can see by simple manipulation of these results, the linear fit is inconsistent with the disparity for which we are looking; at  $y = 230$ , the “disparity” between these two linear fits is  $\Delta E = 0.0046$ , which is about four times smaller than the discontinuity we are looking for. In addition, the amount of error in both linear fits is considerable. This again is due to the large amount of noise variance in the data for energies above the K-edge. The two above methods serve to verify that we simply do not have enough information to find a good linear estimate to the data above the K-edge. This second search for the disparity was as inconclusive as the first.

Although the disparity could not be clearly seen by the above data analysis methods, we can use the histogram of the data near the silicon K-edge in order to find an upper limit to the deviation from linearity for which we are searching. At the 95% confidence level, the upper limit on any deviation from linear gain is equal to twice the value of the standard deviation of a Gaussian fit to the histogrammed data:

Upper limit on deviation from linear gain @ 95% confidence:	$2\sigma = 4.01 \times 10^{-2}$
---	---------------------------------

This means that, according to the analysis, the silicon K-edge disparity within the data is less than this value, to a certainty of 95%.

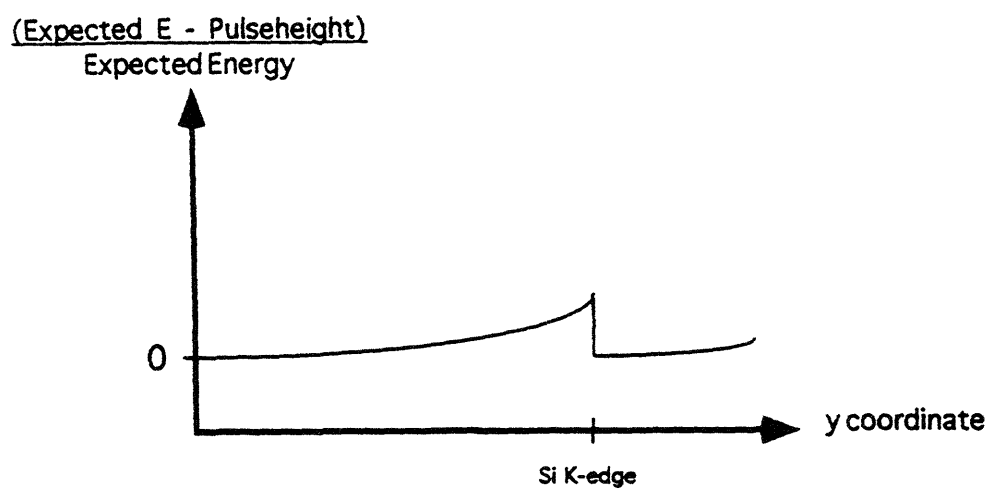


**Figure 3.2.1.** Theoretical expected form of  $\Delta E$  vs.  $y$  plot.

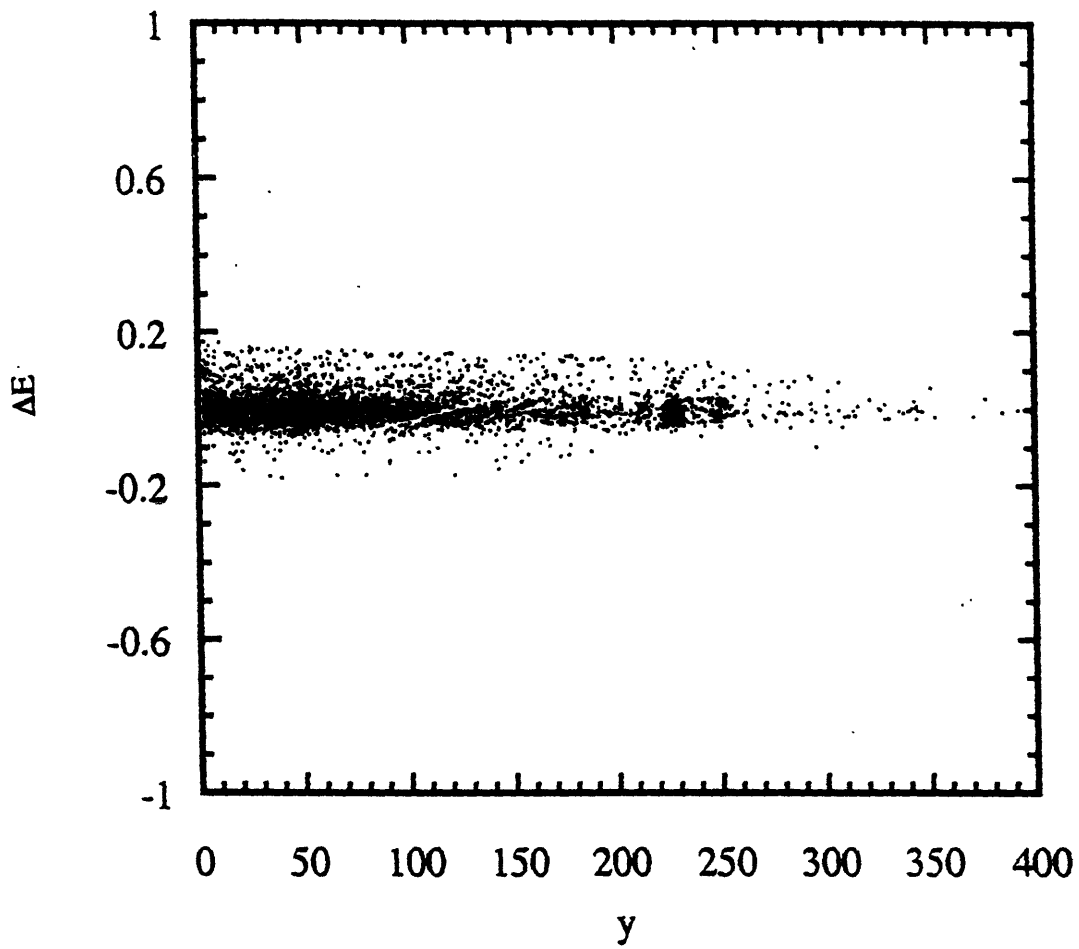


**Figure 3.2.2.**  $\Delta E$  vs.  $y$  for all single event points.



Cumulative Plot of Chop#1,2,3

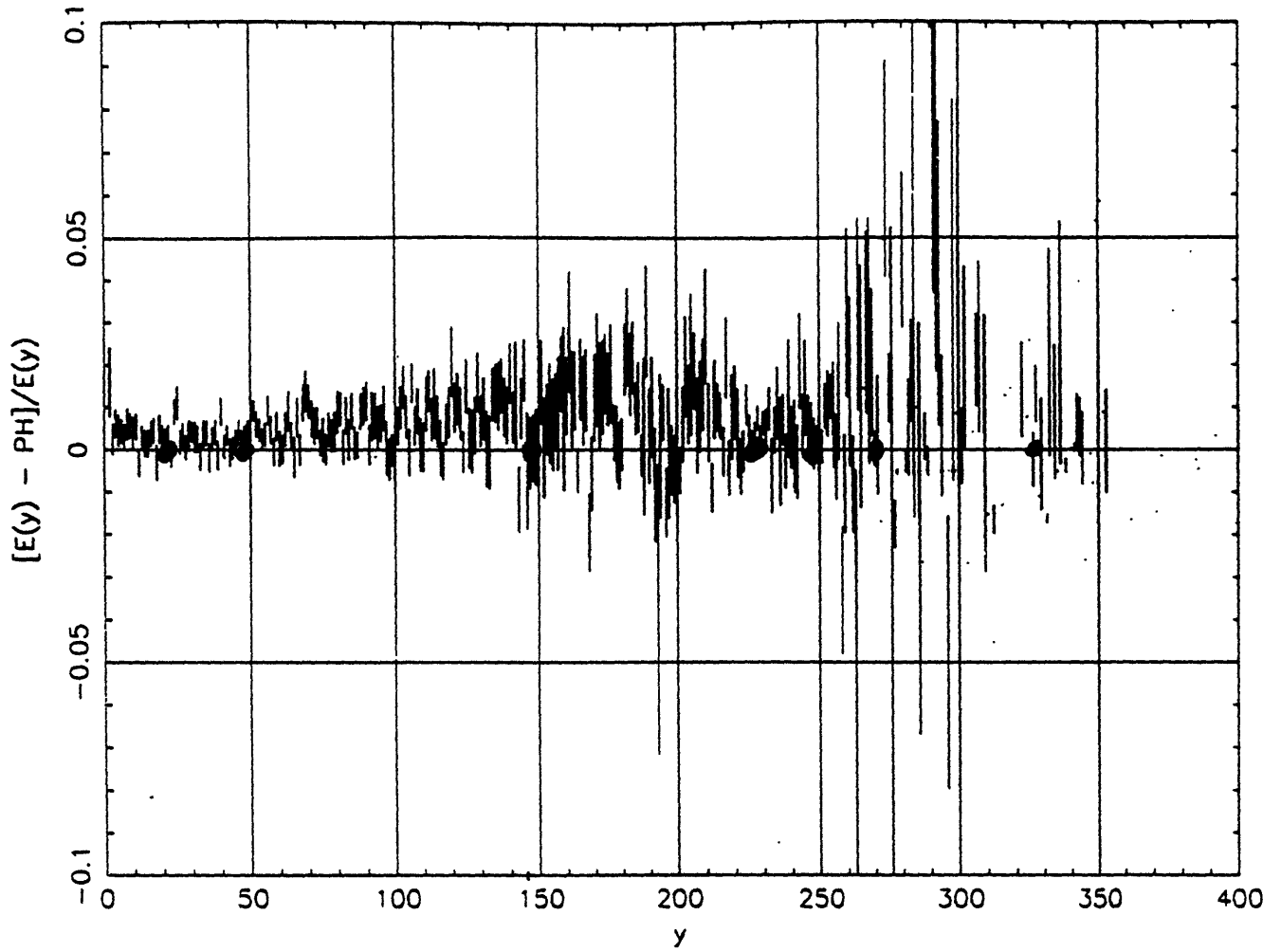


Figure 3.2.3. Cumulative plot of averaged  $\Delta E$  vs.  $y$ , averaged every single  $y$  value.

Cumulative Plot of Chop#1,2,3  
(averaged every 5 y values)

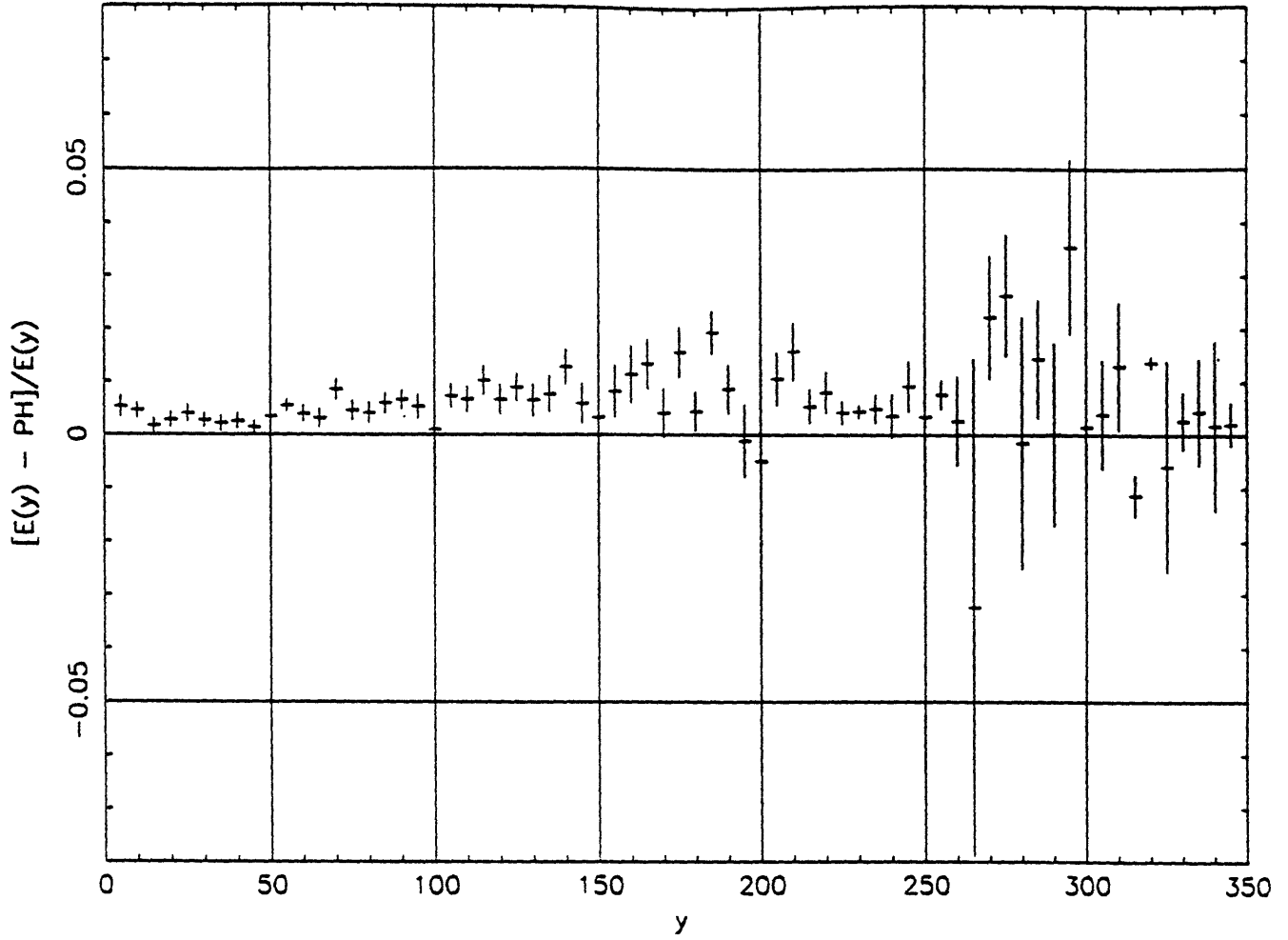


Figure 3.2.4. Cumulative plot of averaged  $\Delta E$  vs.  $y$ , averaged every five  $y$  values.

Cumulative Plot of Chop#1,2,3  
(averaged every 10 y values)

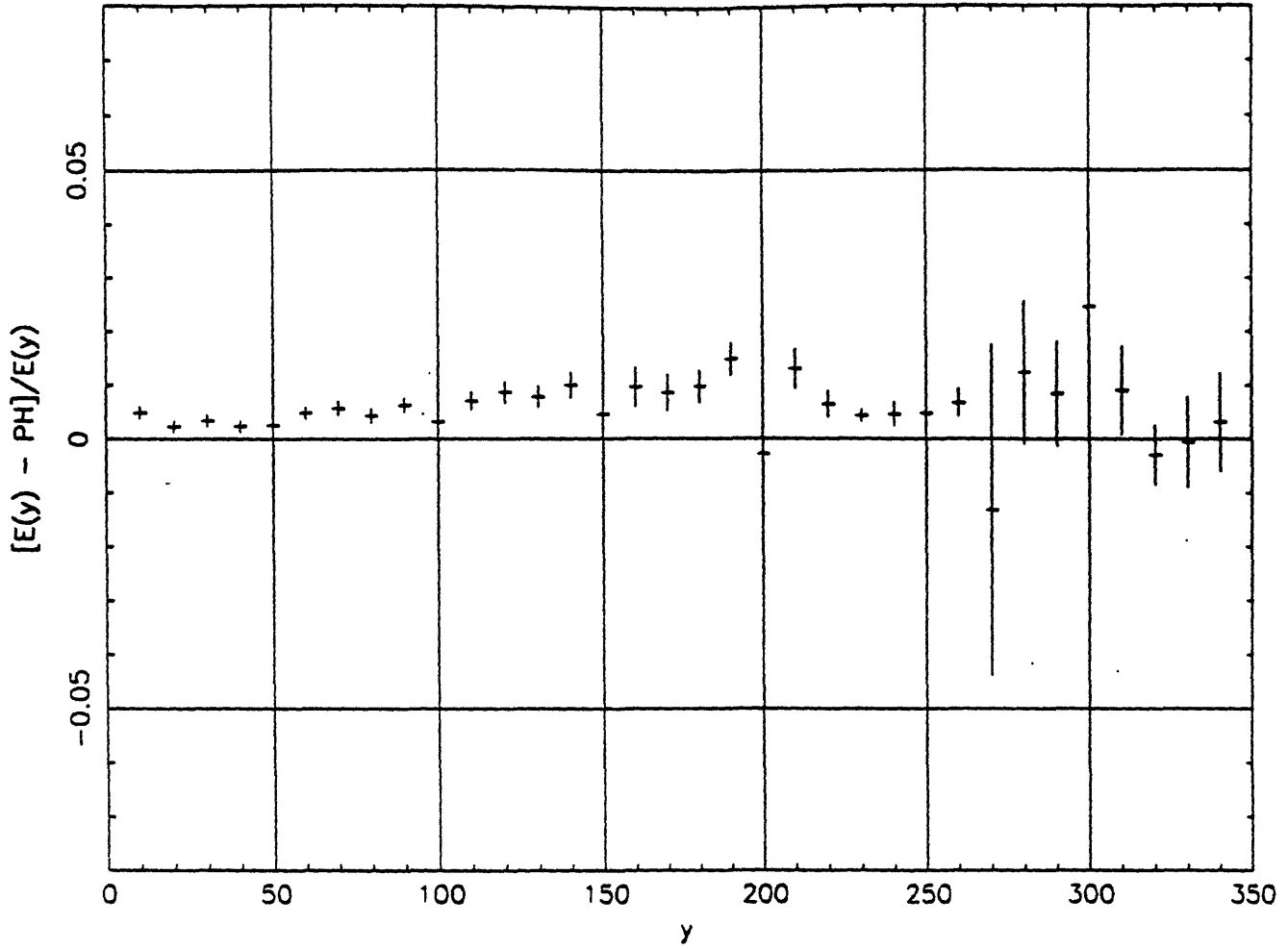
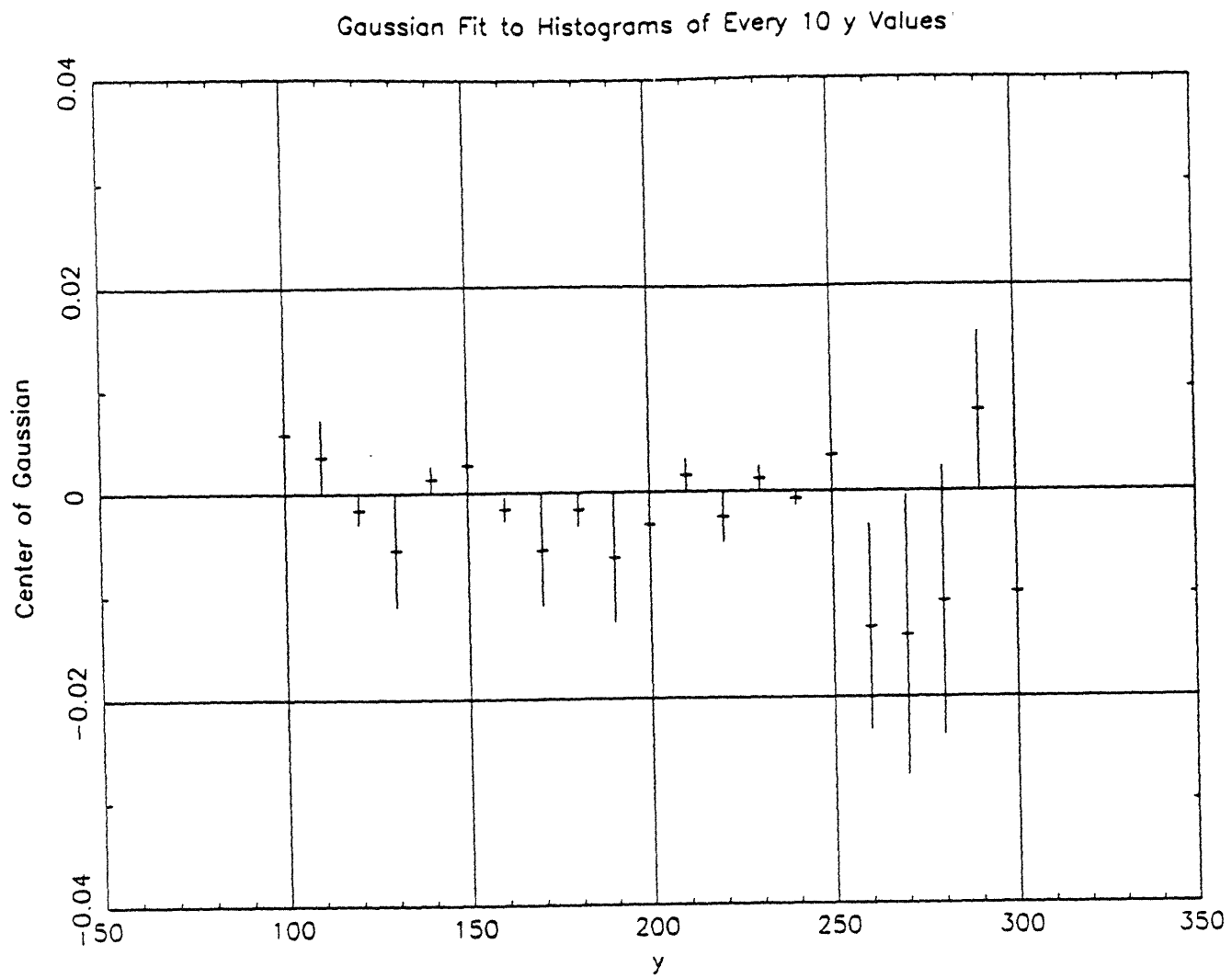


Figure 3.2.5. Cumulative plot of averaged  $\Delta E$  vs.  $y$ , averaged every ten  $y$  values.



**Figure 3.2.6.** Gaussian fit to histograms of every ten y values.

### 3.3 Results of Analysis

The outcome of the final experiment on the SIS CCDs was disappointing. The analysis done was inconclusive, and the variation in the CCD dispersion was not found precisely. What would be necessary for this experiment to result in a more productive conclusion? Ideally, the variation between energy in and pulseheight out must be less than 1% such that the 1 to 2% non-linearity can be detected. In theory, in order to measure a 2% disparity, we need a certain amount of data. With enough data, the error in the data would be less and the disparity would be seen. How many data points are necessary to see the disparity? Taking into consideration the averaging program explained in the last section, we know that

$$\text{Standard Deviation of the Mean} \equiv \sigma_{\mu} = \frac{1}{\sqrt{N}} \cdot \sqrt{\lim_{N \rightarrow \infty} \left[ \frac{1}{N} \sum_i x_i^2 \right] - \mu^2}$$

In order to have a mean standard deviation which is less than the expected disparity, we must have a certain number of points. The number of photons we must have per “averaging bin” (discussed in section 3.2),  $N$ , is directly related to the maximum possible error in energy measurement found in Table 3.2.

$$\frac{\Delta E}{E} = \frac{\sigma_{\mu}}{\mu}$$

$$\frac{\sigma_{\mu}}{\mu} < \frac{0.01}{\text{SNR}} \rightarrow \frac{1}{\mu} \cdot \frac{\sigma}{\sqrt{N}} < \frac{0.01}{\text{SNR}}$$

$$N > [100 \cdot \text{SNR} \cdot \frac{\sigma}{\mu}]^2 \rightarrow N > [100 \cdot \text{SNR} \cdot \frac{\Delta E}{E}]^2$$

**N > 25 photons for 1σ**

**N > 225 photons for 3σ**

etc...

Here, SNR is the signal-to-noise ratio of the data that we desire. In the previous plots, there were about 200 photons per bin in the lower energy ranges. This would allow a most accurate energy measurement of about 3σ. This means that at points near the silicon K-edge energy values (i.e. at higher energies), we need a substantial amount of data per energy value in order to have a small enough standard deviation to see the disparity.

Various errors and experimental limitations may have contributed to the poor final results we obtained. Experimental procedures may have introduced errors which prevented the detection of the disparity. First, a systematic error in the data analysis may have come from the final dispersion solution. Using eight points to fit for four parameters gave four degrees of freedom and a delta chi-squared of approximately 1.5. This signifies that the dispersion solution fit was not arbitrarily precise. Although this systematic error may have altered the final numerical results, it could not have “hidden” a gain disparity at the silicon K-edge. This type of non-linear disparity would not have been masked by an error in a smoothly varying curve.

Another systematic error may have propagated through the data analysis due to the approximate gain calculation. A minimum number of spectral lines were used in the gain calculation, and a first-order averaging approximation was made in order to find a value for the gain. Similar to the above error in the dispersion solution, it is unlikely that this error would have hidden the disparity for which we are searching; however, as was mentioned previously, this error may have resulted in the visible constant offset we see in the  $\Delta E$  vs.  $y$  plots of our final analysis.

A second, more significant error may stem from a main assumption made in the determination of the gain. This assumption was that the value of the gain was constant over all energies. This may not be the case. If we look once again at the identification of eight energy peaks (in Section 3.1), we see that the same line, measured at different places on the detector, does not have the same event pulseheight. For example, the Tungsten line has measured pulseheights of 450.8 in the second order, and 447.5 in the third order. The appearance of non-linearity in the CCD gain may be due to the variation of charge transfer efficiency over the area of the CCD, and this non-linear variation which is on the order of 1% may have contributed to masking the 1 to 2% K-edge disparity.

A final effect, due to the physical nature of silicon, may also have contributed to the masking of the nonlinearity. According to Fraser et. al (1994), there is a discontinuous change in  $W$ , the average energy needed to create an electron-hole pair, at the silicon K-edge. For energies below the K-edge,  $W$  is 3.81 eV/electron. For energies above the edge,  $W$  becomes 3.76 eV/electron. This means that at lower energies, there is a 2% change in the energy required to create the electron-hole pairs of a charge cloud in the CCD. In other words, the average charge cloud size becomes smaller due to the change in  $W$ . However, as we have shown previously, analysis of charge cloud diffusion in the CCD shows that charge cloud spreading increases for energies just below the K-edge. In our analysis, these two effects may “cancel out” in some measure, thereby reducing the size of

the disparity at the silicon K-edge, and in this way decreasing the possibility of identifying it by the mechanism we have used here. The significant systematic errors identified above and the inherent physical properties of the silicon CCD must be studied, analyzed, and quantified to a precise degree in order for a disparity to be visible in the final results.



## Chapter 4

# Conclusion

The ASCA satellite is a considerably advanced X-ray astronomy satellite due to its modern focal plane instruments, the Gas Imaging Spectrometer and the Solid-State Imaging Spectrometers. This research, a study of the Solid-State Imaging Spectrometers on ASCA, was both a theoretical modeling of the behavior of silicon detectors as they interact with x-rays of different energies, and also an investigation into the actual operation of the SIS CCDs.

The theoretical study of silicon based x-ray detectors reveals that a deviation from a nearly linear energy scale may exist near the silicon K-edge. In the SIS CCDs, methods of classification of events, combined with the physical characteristics and behavior of charge clouds within silicon, contribute to a sudden change in the energy in/ output pulseheight relationship at the K-edge. The result of a theoretical analysis of this sudden change shows that a one to two percent deviation between expected CCD output energy and actual CCD pulseheight exists.

If actual SIS CCD data is studied, the main result found is that first, a significant amount of data is needed to see this 1 to 2% disparity, and second, systematic errors must be very carefully accounted for in order to allow the observation of the disparity. Although at this time it seems as though the silicon K-edge disparity does not play a large

role in the performance of the SIS CCD detector, in the future more precise detectors may necessitate and allow the identification and analysis of this non-linearity.

# Appendices

## Appendix A: Results from the Fraser, et al. Calculation

It is interesting to note that Fraser et al. Performed a similar experiment, i.e. a linearity study of silicon in the 0.05 to 8 keV range. It was an investigation into the energy variation of the  $W$  parameter of x rays (that is, the average energy necessary to produce an internal electron-hole pair) in a silicon detector.

The investigating group used microscopic cross-sections of electron interactions to model the creation of secondary electrons by the energy loss from x-ray induced primaries. In addition the group determined the probability of photoelectric absorption by silicon electron shells by a database of atomic cross-sections. From this they found that above the silicon K-edge, at 1839 eV, there is a  $\approx 92\%$  probability of absorption by K-shell electrons. In the region right below the K-edge, the probability of absorption is distributed between the  $L_I$ ,  $L_{II}/L_{III}$ , and  $M_I$  shells.

Fraser, et. al also ran a monte-carlo simulation which did not handle charge diffusion. They calculated  $W$  and  $F$ , the Fano factor, for a number of energies, noting characteristics of temperature and energy dependence. One important observation that is mentioned in the paper is that at energies above the silicon K-edge (specifically 1.3 to 4 keV), the value of  $W$  is 3.76 eV/electron; whereas, at energies below the edge,  $W$  changes discontinuously to 3.81 eV/electron.

The final analysis showed that departures from ideal linearity in the silicon x-ray detector do exist; however, these nonlinearities are likely to be small, at the 1% level.

## Appendix B: Henke Scattering Factors

Low-Energy X-Ray Interaction Coefficients:  
Photoabsorption, Scattering, and Reflection  
E = 30-30,000 eV, Z = 1-92

B.L. Henke, E.M. Gullikson, and J.C. Davis  
Center for X-Ray Optics, 2-400  
Lawrence Berkeley Laboratory  
Berkeley, California 94720

These files were used to generate the tables published in reference [1]. The ascii files contain three columns of data: Energy(eV), f<sub>1</sub>, f<sub>2</sub>, where f<sub>1</sub> and f<sub>2</sub> are the atomic (forward) scattering factors. The data is given on a uniform logarithmic mesh with 301 points from 10 eV to 30,000 eV. (Note: below 30 eV f<sub>1</sub> is set equal to -9999.) the tabulated values of f<sub>1</sub> contain a relativistic, energy independent, correction given by,  $Z^* = Z - (z/82.5)^{(2.37)}$ .

The atomic photoabsorption cross section, mu<sub>a</sub>, may be readily obtained from the values of f<sub>2</sub> using the relation,

$$\mu_a = 2*r_0*\lambda*f_2$$

where r<sub>0</sub> is the classical electron radius, and lambda is the wavelength. The index of refraction for a material with N atoms per unit volume is calculated by,

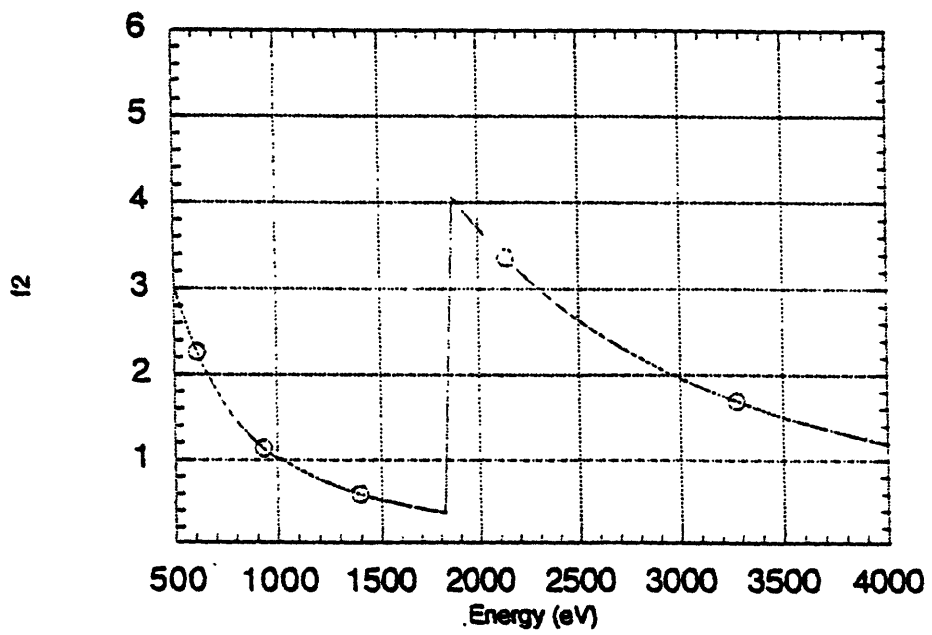
$$n = 1 - N*r_0*(\lambda)^2*(f_1+if_2)/(2*\pi).$$

These (semi-empirical) atomic scattering factors are based upon photoabsorption measurements of elements in their elemental state. The basic assumption is that condensed matter may be modeled as a collection of non-interacting atoms. This assumption is in general a good one for energies sufficiently far from absorption thresholds. In the threshold regions, the specific chemical state is important and direct experimental measurements must be made.

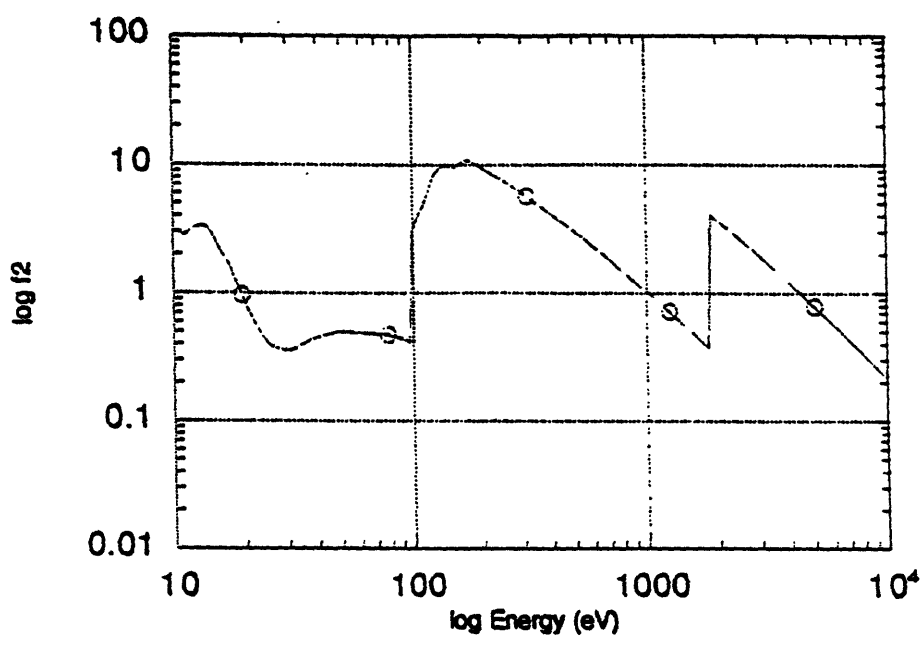
These tables are based on a compilation of the available experimental measurements and theoretical calculations. For many elements there is little or no published data and in such cases it was necessary to rely on theoretical calculations and interpolations across Z. In order to improve the accuracy in the future considerably more experimental measurements are needed.

[1] B.L. Henke, E.M. Gullikson, and J.C. Davis, Atomic Data and Nuclear Data Tables Vol. 54 No. 2 (July 1993).

Linear Plot of  $f_2$  Scattering Factor for Silicon in Region of Silicon K-Edge



log-log plot of Henke  $f_2$  scattering factor for Silicon



## Appendix C: Filtering and Rotation programs

```
rotate_zero.c      Tue Nov 30 13:25:20 1993      1
/* rotate_zero.c   Written November 1993   Srimal Wangu

   This program takes an angle theta, in radians, a point of origin,
   and an input evlist, and rotates the input list by the given angle
   ABOUT THE ORIGIN, putting the result into 'rotated.evlist'
*/

#include <stdio.h>
#include <math.h>
#include "rv.h"

struct data_str eventdata;

main(argc,argv)
int argc;
char *argv[];
{
    float theta,xtemp;
    int sum,x,y;
    if (argc==2) theta=atof(argv[1]);
    else
    {
        fprintf(stderr,"read the manual stupid!!");
    }
    while (read(0,&eventdata,datastr_size) == datastr_size)
    {
        xtemp = (eventdata.x*cos(theta) + eventdata.y*sin(theta));
        eventdata.y = (short)(-eventdata.x*sin(theta) + eventdata.y*cos(theta));
        eventdata.x = (short)(xtemp);
        write(1,&eventdata,datastr_size);
    }
    exit(0);
}
```

```

rotate.c      Wed Dec 1 16:40:13 1993      1

/* rotate.c   Written November 1993   Srimal Wangu

   This program takes an angle theta, in radians, a point of origin,
   and an input evlist, and rotates the input list by the given angle
   ABOUT A GIVEN Xo and Yo, putting the result into 'rotated.evlist'
*/

#include <stdio.h>
#include <math.h>
#include "rv.h"

struct data_str eventdata;

main(argc,argv)
int argc;
char *argv[];
{
    float theta,xtemp,ytemp;
    int sum,x,y,xo,yo;
    if (argc==4)
        {theta=atof(argv[1]);
         xo=atof(argv[2]);
         yo=atof(argv[3]);}
    else
        {
            fprintf(stderr,"read the manual stupid!!");
        }
    while (read(0,&eventdata,datastr_size) == datastr_size)
        {
            xtemp = ((eventdata.x - xo)*cos(theta) + (eventdata.y - yo)*sin(theta));

            ytemp = (short)(-(eventdata.x - xo)*sin(theta)+(eventdata.y - yo)*cos(theta));

            eventdata.x = (short)(xtemp+xo);
            eventdata.y = (short)(ytemp+yo);
            write(1,&eventdata,datastr_size);
        }
    exit(0);
}

```

listeventdata.c      Wed Feb 2 16:52:00 1994      1

/\* listeventdata.c    written January 28, 1994    Srimal Wangu

This module takes the event data stream from any file.swlist and displays the data in columns with the format:

```
x y # of events in 9 surrounding pixels sum of events
- - -----
```

NOTE: I DONT KNOW WHAT TO ASSUME FOR DARK\_FB\_MULT, SO I'M ASSUMING IT TO BE 1

\*/

#include "rv.h"

struct data\_str eventdata;

main(argc,argv)

int argc;

char \*argv[];

```
{
  short i,count,DARK_FB_MULT,DARK_FB_BITS,preamble;
  int sum,x,y,pream_size;
```

```
  count = 0;
  read(0,&preamble,pream_size);
  while(read(0,&eventdata,datastr_size) == datastr_size)
```

```
  {
    sum = 0;
    if (argc == 2)
    {
      x = eventdata.x;
      y = eventdata.y;
      printf("%d\t%d\t%d\t%d\n",++count,x,y,eventdata.data[4]/DARK_FB_MULT);
      printf("\t%d\t%d\t%d\n",x-1,y-1,eventdata.data[0]/DARK_FB_MULT);
      printf("\t%d\t%d\t%d\n",x,y-1,eventdata.data[1]/DARK_FB_MULT);
      printf("\t%d\t%d\t%d\n",x+1,y-1,eventdata.data[2]/DARK_FB_MULT);
      printf("\t%d\t%d\t%d\n",x-1,y,eventdata.data[3]/DARK_FB_MULT);
      printf("\t%d\t%d\t%d\n",x+1,y,eventdata.data[5]/DARK_FB_MULT);
      printf("\t%d\t%d\t%d\n",x-1,y+1,eventdata.data[6]/DARK_FB_MULT);
      printf("\t%d\t%d\t%d\n",x,y+1,eventdata.data[7]/DARK_FB_MULT);
      printf("\t%d\t%d\t%d\n",x+1,y+1,eventdata.data[8]/DARK_FB_MULT);
    }
```

```
  }
  else
  {
    printf("%d\t%d",eventdata.x,eventdata.y);
    for(i=0;i<9;i++)
    {
      sum += eventdata.data[i]>>DARK_FB_BITS;
      printf("\t%d.1f",((float)eventdata.data[i]));
    }
    printf("\t%d\n",sum);
  }
}
```



```

lineselect.c      Fri Feb 11 11:22:04 1994      1

/* lineselect.c  written February, 1994  Srimal Wangu

   Program to "filter out" 1 line from a CCD spectrum, given ymin,ymax, and
   a pulse threshold value;
   Takes data from a listevents file
*/

#include <stdio.h>
#include "rv.h"

main(argc,argv)
int argc;
char *argv[];
{
  int ymin,ymax,threshold,x,y,sum;
  float ev1,ev2,ev3,ev4,ev5,ev6,ev7,ev8,ev9;
  char *filename;
  FILE *f;

  if (argc==5)
  {
    filename = argv[1];
    ymin = atoi(argv[2]);
    ymax = atoi(argv[3]);
    threshold = atoi(argv[4]);
  }
  else
  {
    printf("Usage: lineselect <file.listevents> <ymin> <ymax> <threshold>\n");
    exit();
  }

  f = fopen(filename,"r");

  if (f==NULL)
  {
    printf("Open of %s for input failed (doesn't exist)\n",filename);
    exit();
  }

  while ( fscanf(f, "%d\t%d\t%f\t%f\t%f\t%f\t%f\t%f\t%f\t%f\t%f\t%d\t\n",
    OF)
    &x, &y, &ev1, &ev2, &ev3, &ev4, &ev5, &ev6, &ev7, &ev8, &ev9, &sum) != E
  {
    if ( (y>=ymin) && (y<=ymax) && (sum >= threshold) )
      printf("%d\t%d\t%f\t%f\t%f\t%f\t%f\t%f\t%f\t%f\t%f\t%d\n",x,y,ev1,
        ev2,ev3,ev4,ev5,ev6,ev7,ev8,ev9,sum);
  }
}

```

```

regionselect.c      Fri Feb 11 11:20:57 1994      1

/* regionselect.c  written February, 1994  Srimal Wangu

   Program to "filter out" a region from a CCD spectrum, given ymin and ymax:
   Takes data from a listevents file
*/

#include <stdio.h>
#include "rv.h"

main(argc,argv)
int argc;
char *argv[];
{
    int ymin,ymax,x,y,sum;
    float ev1,ev2,ev3,ev4,ev5,ev6,ev7,ev8,ev9;
    char *filename;
    FILE *f;

    if (argc==4)
    {
        filename = argv[1];
        ymin = atoi(argv[2]);
        ymax = atoi(argv[3]);
    }
    else
    {
        printf("Usage: regionselect <file.listevents> <ymin> <ymax>\n");
        exit();
    }

    f = fopen(filename,"r");

    if (f==NULL)
    {
        printf("Open of %s for input failed (doesn't exist)\n",filename);
        exit();
    }

    while ( fscanf(f, "%d\t%d\t%f\t%f\t%f\t%f\t%f\t%f\t%f\t%f\t%f\t%d\t\n",
        &x, &y, &ev1, &ev2, &ev3, &ev4, &ev5, &ev6, &ev7, &ev8, &ev9, &sum) != E
OF)
    {
        if ( (y>=ymin) && (y<=ymax) )
            printf("%d\t%d\t%f\t%f\t%f\t%f\t%f\t%f\t%f\t%f\t%f\t%d\t\n",x,y,ev1,
                ev2,ev3,ev4,ev5,ev6,ev7,ev8,ev9,sum);
    }
}

```

## Appendix D: Averaging Programs

```
/* This program takes in a file, and gives the averages for all the different y's. */
#include <stdio.h>
#include <math.h>

const MAXNUM = 400;
char *READ_FILE = "m3_123.sorted";
char *WRITE_FILE = "123_all_5";

main()
{
    FILE *fp,
        *fp2;
    char c;
    int num,
        y,
        one,
        two,
        three,
        four,
        five,
        six,
        seven,
        eight,
        nine,
        ten,
        eleven,
        y0,
        five_check;
    float sum,
        sumsqr,
        avg,
        diff,
        exptd,
        uncert;

    Boolean lookup_y;

    sum = 0;
    sumsqr = 0;
    num = 0;
    y0 = 2;
    fp = fopen( READ_FILE, "r" );
    fp2 = fopen( WRITE_FILE, "w" );
    lookup_y = TRUE;

    while ( y0 <= MAXNUM )
    {
        if ( lookup_y )
        {
            while ( ( c = fgetc( fp ) ) != '\t' )
            ;
            fscanf( fp, "%d\t", &y );
        }
        if ( y == y0 )
        {
            fscanf( fp, "%d\t%d\t%d\t%d\t%d\t%d\t%d\t%d\t%d\t%d\t%f\t%f", &one, &two,
                &three, &four, &five, &six, &seven, &eight, &nine, &ten, &sexptd, &diff );
        }
    }
}
```

```

sum += diff;
sumsq += diff*diff;
num++;
lookup_y = TRUE;
}
else
{
five_check = y0 % 5;
if ( !five_check )
{
if ( num )
{
avg = sum / num;
uncert = sqrt( ( ( sumsq / num ) - ( avg*avg ) ) / num );
}
else
{
avg = 0;
uncert = 0;
}
printf( "Finished y = %d...\n", y0 );
fprintf( fp2, "%d\t%f\t%f\n", y0, avg, uncert );
sum = 0;
num = 0;
sumsq = 0;
}
y0++;
lookup_y = FALSE;
}
}
fclose( fp );
fclose( fp2 );
}

```

```

/* This program takes in a file, and gives the averages for all the different y's. */

#include <stdio.h>
#include <math.h>

const MAXNUM = 400;
char *READ_FILE = "m3_123.sorted";
char *WRITE_FILE = "123_all_10";

main()
{
    FILE *fp,
        *fp2;
    char c;
    int num,
        y,
        one,
        two,
        three,
        four,
        five,
        six,
        seven,
        eight,
        nine,
        ten,
        eleven,
        y0,
        five_check;
    float sum,
        sumsqr,
        avg,
        diff,
        exptd,
        uncert;

    Boolean lookup_y;

    sum = 0;
    sumsqr = 0;
    num = 0;
    y0 = 2;
    fp = fopen( READ_FILE, "r" );
    fp2 = fopen( WRITE_FILE, "w" );
    lookup_y = TRUE;

    while ( y0 <= MAXNUM )
    {
        if ( lookup_y )
        {
            while ( ( c = fgetc( fp ) ) != '\t' )
                ;
            fscanf( fp, "%d\t", &y );
        }
        if ( y == y0 )
        {
            fscanf( fp, "%d\t%d\t%d\t%d\t%d\t%d\t%d\t%d\t%d\t%d\t%f\t%f", &one, &two,
                &three, &four, &five, &six, &seven, &eight, &nine, &ten, &exptd, &diff);
        }
    }
}

```

```

sum += diff;
sumsq += diff*diff;
num++;
lookup_y = TRUE;
}
else
{
five_check = y0 % 10;
if ( !five_check )
{
if ( num )
{
avg = sum / num;
uncert = sqrt( ( (sumsq / num ) - (avg * avg ) ) / num );
}
else
{
avg = 0;
uncert = 0;
}
printf( "Finished y = %d...\n", y0 );
fprintf( fp2, "%d\t%f\t%f\n", y0, avg, uncert );
sum = 0;
num = 0;
sumsq = 0;
}
y0++;
lookup_y = FALSE;
}
}
fclose( fp );
fclose( fp2 );
}

```

```
/* This program takes in a file, and gives the averages for all the different y's. */
```

```
#include <stdio.h>
```

```
#include <math.h>
```

```
const MAXNUM = 400;
```

```
char *READ_FILE = "m3_123.sorted";
```

```
char *WRITE_FILE = "123_all_1";
```

```
main()
```

```
{
```

```
FILE *fp,
```

```
*fp2;
```

```
char c;
```

```
int num,
```

```
y,
```

```
one,
```

```
two,
```

```
three,
```

```
four,
```

```
five,
```

```
six,
```

```
seven,
```

```
eight,
```

```
nine,
```

```
ten,
```

```
eleven,
```

```
y0,
```

```
five_check;
```

```
float sum,
```

```
sumsqr,
```

```
avg,
```

```
diff,
```

```
exptd,
```

```
uncert;
```

```
Boolean lookup_y;
```

```
sum = 0;
```

```
sumsqr = 0;
```

```
num = 0;
```

```
y0 = 2;
```

```
fp = fopen( READ_FILE, "r" );
```

```
fp2 = fopen( WRITE_FILE, "w" );
```

```
lookup_y = TRUE;
```

```
while ( y0 <= MAXNUM )
```

```
{
```

```
if ( lookup_y )
```

```
{
```

```
while ( ( c = fgetc( fp ) ) != '\t' )
```

```
;
```

```
fscanf( fp, "%d\t", &y );
```

```
}
```

```
if ( y == y0 )
```

```
{
```

```
fscanf( fp, "%d\t%d\t%d\t%d\t%d\t%d\t%d\t%d\t%d\t%d\t%f\t%f",
```

```
&one, &two, &three, &four, &five, &six, &seven, &eight, &nine, &ten,
```

```

    sexptd, adiff );
    sum += diff;
    sumsqr += diff * diff;
    num++;
    lookup_y = TRUE;
}
else
{
    if ( num )
    {
        avg = sum / num;
        uncert = sqrt( ( ( sumsqr / num ) - ( avg * avg ) ) / num );
    }
    else
    {
        avg = 0;
        uncert = 0;
    }
    printf( "Finished y = %d...\n", y0 );
    fprintf( fp2, "%d\t%f\t%f\n", y0, avg, uncert );
    sum = 0;
    num = 0;
    sumsqr = 0;
    y0++;
    lookup_y = FALSE;
}
}
fclose( fp );
fclose( fp2 );
}

```



## References

Adams, D.J. Cosmic X-Ray Astronomy. Bristol, U.K.: Monographs on Astronomical Subjects (6), 1980.

Astro-D Technical Description: AO-1 Version. December 15, 1992.

Astro-D Technical Description: AO-3 Version. July 29, 1994.

Bautz, Mark. Simplified Estimate of Distribution of X-Ray Induced Charge Cloud Sizes. Astro-D Memo #465. November 20, 1992.

Bautz, Mark. SIS CCD Structure. Astro-D Memo #427. June 29, 1992.

Bekefi, George, and Alan H. Barrett. Electromagnetic Vibrations, Waves, and Radiation. Cambridge, MA: MIT Press, 1977.

Bertin, Eugene P. Introduction to X-Ray Spectrometric Analysis. New York: Plenum Press, 1978.

Bevington, Philip R. and D. Keith Robinson. Data Reduction and Error Analysis for the Physical Sciences. New York: McGraw-Hill, Inc., 1992.

Center for X-Ray Optics: X-Ray Data Booklet. Ed. Douglas Vaughan. Berkeley, CA: Lawrence Berkeley Laboratory, 1986.

Compton, Arthur H. X-Rays in Theory and Experiment. New York: D.Van Nostrand Co., Inc., 1935.

Encyclopædia Britannica, 15th ed. (1983) S.v. "Atomic Structure," "Semiconductors," "Spectroscopy," "X-Ray Astronomy," "X-Rays".

Fraser, G.W. X-Ray Detectors in Astronomy. New York: Cambridge University Press, 1989.

Fraser, G.W. et al. "The X-Ray Energy Response of Silicon: (A) Theory". Nucl. Inst. Meth. Phys.Res.A. June, 1994.

HIREFS Spectrometer Operating Instructions. Hettrick Scientific, Inc. October 22, 1990.

Hollas, J. Michael. Modern Spectroscopy, Second Edition. New York: John Wiley & Sons Ltd., 1992.

Inoue, H. "The Astro-D Mission." Advances in Space Research, vol.11, no.8, pp.259-264, 1991.

Inoue, H. "The X-Ray Astronomy Satellite 'ASCA'." Experimental Astronomy. 4:1-10, 1993.

Michette, A.G. and C.J. Buckley, eds. X-Ray Science and Technology. Philadelphia: Institute of Physics Publishing, 1993.

Sze, S.M. Properties of Semiconductor Devices. New York: John Wiley & Sons, 1969.

Tanaka, Y. "The Astro-D Mission." Advances in Space Research, vol.10, no.2,  
pp.255-260, 1990.

Tucker, Wallace and Riccardo Giacconi. The X-Ray Universe. Cambridge, MA: Harvard  
University Press, 1985.

Wenham, E.J., et al. Physics: Concepts and Models. Reading, Massachusetts: Addison-  
Wesley Publishers, 1972.

"X-Ray Timing Explorer: Taking the Pulse of the Universe" (Information Booklet), 1993.